



Spectra and Anisotropy of Solar Energetic Protons During GLE #65 on 28 October, 2003 and GLE #66 on 29 October, 2003

Alexander L. Mishev^{1,2} · Sergey A. Koldobskiy^{1,2} · Nicholas Larsen² · Ilya G. Usoskin^{1,2}

Received: 5 December 2023 / Accepted: 31 January 2024
© The Author(s) 2024

Abstract

Solar Cycle 23 was the most active in ground-level enhancements (GLEs) with 16 events registered by the global neutron monitor network. In this paper, we study a very active period in October–November, 2003, which revealed an intense solar activity burst that led to several eruptive processes and produced a sequence of three GLEs. By applying state-of-the-art modelling to records from the global neutron monitor network as well as space-borne data, we derived the spectral and anisotropy characteristics of accelerated solar protons during the GLE #65 event on 28 October, 2003 and GLE #66 on 29 October, 2003. The spectra and the pitch angle distributions are obtained with a 5-min time resolution, providing their dynamical evolution throughout the event. The spectra are parameterised with a modified power-law rigidity spectrum, whilst the angular distribution with a Gaussian. The constraints and uncertainties of the derived characteristics are evaluated by corresponding modelling.

Keywords Ground level enhancement · Neutron monitor · Data analysis · Solar energetic particles

1. Introduction

Manifestations of powerful solar activity processes, namely major solar eruption(s), such as solar flares and coronal mass ejections (CMEs), can result in the acceleration of solar ions up to relativistic energies (e.g., Desai and Giacalone, 2016; Anastasiadis et al., 2019). The accelerated to high energies solar ions are known as solar energetic particles (SEPs).

✉ A.L. Mishev
alexander.mishev@oulu.fi; alex_mishev@yahoo.com

S.A. Koldobskiy
sergey.koldobskiy@oulu.fi

N. Larsen
nicholas.larsen@oulu.fi

I.G. Usoskin
ilya.usoskin@oulu.fi

¹ Sodankylä Geophysical Observatory, University of Oulu, Oulu, Finland

² Space Physics and Astronomy Research Unit, University of Oulu, Oulu, Finland

Their energy in most cases is in the deka-MeV range, yet ions can be accelerated up to 100 MeV/n energy range. Occasionally, several times per solar cycle with higher probability during the solar maximum and the decline phase of the solar cycle (for details see Shea and Smart, 2000; Papaioannou et al., 2016), SEPs can be accelerated to the GeV/n range (e.g., Aschwanden, 2012; Reames, 2013; Desai and Giacalone, 2016, and references therein). In such cases, solar ions induce a complicated particle cascade in the Earth's atmosphere, so that the secondary particles can be registered on the ground by convenient detectors such as neutron monitors (NMs – see, e.g., Hatton, 1971; Simpson, 2000; Dorman, 2006, and references therein). This specific class of events is called ground-level enhancements (GLEs – see, e.g., Shea and Smart, 1982; Stoker, Dorman, and Clem, 2000; Poluianov et al., 2017).

At the time of writing this paper, the number of registered GLEs was 73, and the first ones, namely GLEs 1–4 were observed in 1942–1949 by ionisation chambers (Forbush, 1946; Forbush, Stinchcomb, and Schein, 1950). Starting from 1956, the global neutron monitor (NM) network is the standard multi-instrument, which allows one to derive important features of GLEs, such as spectra and anisotropy (Simpson, Fonger, and Treiman, 1953; Simpson, 1957; Forbush, 1958; Hatton and Carmichael, 1964; Mavromichalaki et al., 2011). The global NM network is sensitive to primary SEPs with the energy above ≈ 300 MeV/n or 433 MeV/n for the high-mountain polar region and sea-level NMs, respectively (for details, see Mishev and Poluianov, 2021).

The global NM network exploits the geomagnetosphere as a giant spectrometer (Debrunner et al., 1988; Bütikofer et al., 2009), employing the different NM sensitivity over the arrival direction(s) of SEPs and energy range, because stations are located at different geographic locations, correspondingly characterised by the asymptotic directions and rigidity cut-off vs. the impinging proton. Using convenient modelling of the global NM network response, it is possible to study GLEs (see Section 2). We note that the records from the global NM network during GLEs are available, in the standard verified form, in the international GLE database (gle.oulu.fi, Usoskin et al., 2015) or as raw data from the NM data base NMDB (nmdb.eu, e.g., Mavromichalaki et al., 2011).

Naturally, the characteristics of GLEs such as energy spectra, anisotropy, duration, conditions related to geomagnetic and interplanetary transport, as well as the time evolution, vary between the events (Gopalswamy et al., 2012; Miroshnichenko, 2018; Moraal and McCracken, 2012; Raukunen et al., 2018). This usually leads to a study of GLEs on a case-by-case basis. For the present study, we consider an interesting period of October–November, 2003, revealing intense solar activity characterised by several eruptive processes on the Sun producing a sequence of three GLEs. Here we focus on the first and second of the so-called Halloween events, namely the GLE #65 event on 28 October, 2003 and poorly studied GLE #66 on 29 October, 2003 (e.g., Balabin, 2023), in the framework of our study of the bulk of GLEs using the same model and methods; for details, see Section 2. Using the records from the global NM network, we derived the spectra and anisotropy characteristics of both events with unprecedented time resolution.

2. Modelling the NM Response and Analysis of GLE

In order to derive the spectra and anisotropy of SEPs in the energy range ~ 0.3 –20 GeV/n, we employed a method based on modelling of the global NM response (Mishev, Kocharov, and Usoskin, 2014). The method is adapted from the scheme initially proposed by Cramp et al. (1997) and further developed by Bombardieri et al. (2006) and Vashenyuk et al. (2006). A detailed description of the method and several applications are given elsewhere (Mishev

et al., 2018, 2021a,b). The modelling of the global NM response and subsequent unfolding of the spectra includes: computation of geomagnetic rigidity cut-offs and asymptotic directions of all NMs used for the analysis of the event, namely by computation of SEP trajectories in a model magnetosphere (e.g., Smart, Shea, and Flückiger, 2000; Bütikofer, 2018); considering a convenient initial guess of the inverse problem by assuming the apparent source position along the interplanetary magnetic field (IMF) line derived from space-borne measurements (Mishev and Usoskin, 2016b; Kocharov et al., 2017) if available or following Cramp, Humble, and Duldig (1994); and a least squares optimisation of the difference between experimental and modelled NM responses. The fit quality is determined by the residual (e.g., Himmelblau, 1972) given by

$$\mathcal{D} = \frac{\sqrt{\sum_{i=1}^m \left[\left(\frac{\Delta N_i}{N_i} \right)_{\text{mod}} - \left(\frac{\Delta N_i}{N_i} \right)_{\text{meas}} \right]^2}}{\sum_{i=1}^m \left(\frac{\Delta N_i}{N_i} \right)_{\text{meas}}}, \quad (1)$$

where $\left(\frac{\Delta N_i}{N_i} \right)_{\text{mod}}$ and $\left(\frac{\Delta N_i}{N_i} \right)_{\text{meas}}$ (see Equation 2) are the modelled and measured relative count rate increases of the i th station, respectively, and m is the number of the stations used in the analysis.

According to our experience, good convergence of the optimisation, robust solution and reliable description of the experimental data are achieved when $\mathcal{D} \leq 5\% - 10\%$ for strong and moderately strong events (Vashenyuk et al., 2006; Mishev and Usoskin, 2016a, 2018), though for weak and/or highly fluctuated events occurring, e.g., during complicated (disturbed) magnetospheric and/or IMF conditions, \mathcal{D} could be $\approx 15\% - 20\%$ (e.g., Dennis and Schnabel, 1996; Mishev et al., 2018). The minimum value of \mathcal{D} , along with additional criteria, namely uniform distribution of the residuals, the relative difference between the observed and calculated NM increases of the order of about 10%–15% for each NM, as well as the value of $\chi_r^2 = \chi^2/\text{DoF}$ close to unity, where DoF is the number of degrees of freedom, provides the necessary basis to obtain a reliable and robust solution of the inverse problem (Dennis and Schnabel, 1996; Aster, Borchers, and Thurber, 2005).

The method was recently validated (Koldobskiy et al., 2019a) using direct space-borne measurements by the PAMELA (Payload for Antimatter Matter Exploration and Light-nuclei Astrophysics) experiment (Bruno et al., 2018). Herein, the modelling of the NM responses was performed employing a new-generation NM yield function (Mishev et al., 2020), which is in very good agreement with space-borne data and latitude surveys (e.g., Gil et al., 2015; Nuntiyakul et al., 2018), besides it was calibrated using PAMELA (Adriani et al., 2017) and AMS-02 (Alpha Magnetic Spectrometer – Aguilar et al., 2021) data (for details, see Koldobskiy et al., 2019a; Koldobskiy and Mishev, 2022, and the discussion therein). The optimisation is based on the Levenberg–Marquardt method (Levenberg, 1944; Marquardt, 1963) and also includes algorithms developed later (Tikhonov et al., 1995; Mavrodiiev, Mishev, and Stamenov, 2004; Mishev, Mavrodiiev, and Stamenov, 2005), leading to robust unfolding of the spectrum (Aster, Borchers, and Thurber, 2005). The method was used for the analysis of several GLEs including the most recent one GLE#73 in October 2021 (Mishev et al., 2022; Papaioannou et al., 2022).

During the modelling of the global NM response, it is necessary to reproduce count-rate increases of not only NMs with maximal and significant response but also those of NMs with marginal or null responses (for details, see Cramp et al., 1997). In general, the relative count rate increase of an NM at a given moment t is defined as the ratio between the NM count rates due to SEPs and GCRs, the latter averaged over two hours before the

event onset (e.g., Usoskin et al., 2015), and taking into account the contribution of obliquely arriving SEPs, particularly important for modelling strong and/or with complicated angular distribution events (Clem, 1997), is expressed as

$$\frac{\Delta N(P_{\text{cut}})}{N(t)} = \frac{\frac{1}{k} \sum_k \int_{P_{\text{cut}}}^{P_{\text{max}}} J_{\text{sep}}(P, t) S_k(P) G(\alpha(t)) A_k(P) dP}{\sum_i \int_{P_{\text{cut}}}^{\infty} J_{\text{GCR}_i}(P, t) S_i(P) dP}, \quad (2)$$

where $\Delta N(P_{\text{cut}})$ is the count rate increase due to SEPs, $N(t)$ is the background due to GCR, J_{sep} is the rigidity spectrum of SEPs, $J_{\text{GCR}_i}(P, t)$ is the rigidity spectrum of the i th component (proton or α -particle, etc.) of GCR at a given time t , $G(\alpha)$ is the pitch angle distribution (PAD). We emphasize that for GCRs, the angular distribution is assumed to be isotropic (Beatty, Matthews, and Wakely, 2018); $A(P)$ is a discrete function with $A(P) = 1$ and 0 for allowed and forbidden trajectories, respectively (Cooke et al., 1991), as computed for the particle propagation in the geomagnetosphere; P_{cut} is the minimum rigidity cut-off of the station, while P_{max} is the maximum rigidity of SEPs considered in the model (20 GV), whilst for GCR $P_{\text{max}} = \infty$. Furthermore, S_k is the NM yield function, which accounts for obliquely incident SEPs, i.e., from various segments k (for details, see Figure 4 in Cramp et al., 1997, and Figure 3 in Mishev, 2023). In the case of $k = 1$, only vertical SEP arrival is considered and the isotropic yield function is employed for the modelling, still producing reasonable results (Cramp, Humble, and Duldig, 1994; Vashenyuk et al., 2006; Mishev and Usoskin, 2016a). In Equation 2, the GCR spectrum is parameterised by the force-field model (Caballero-Lopez and Moraal, 2004; Usoskin et al., 2005), considering all species, using the local interstellar spectrum (LIS) by Vos and Potgieter (2015), and the modulation potential according to Usoskin et al. (2017). We note that nuclei with atomic number $Z > 2$ are scaled to α -particles (details are given in Usoskin and Kovaltsov, 2006; Mishev and Velinov, 2011; Koldobskiy et al., 2019a). We emphasise that employment of different LIS would not alter the analysis, considering the reported linear relation between the modulation potential values for different parameterisations of LIS (e.g., Usoskin et al., 2005; Herbst et al., 2010; Usoskin et al., 2017; Engelbrecht et al., 2022; Väisänen et al., 2023).

3. Experimental Data of NMs During GLE #65 and GLE #66

Solar cycle 23 started in 1996 and ended in 2008, and revealed notable solar activity, leading to 16 GLEs, including the second strongest recorded GLE #69 on 20 January, 2005 and a sequence of three so-called Halloween events GLE #65–67 in October–November, 2003 (Bütikofer et al., 2009; Andriopoulou et al., 2011a,b; Gopalswamy et al., 2012; Moraal and McCracken, 2012).

The first Halloween event GLE #65 occurred on 28 October, 2003. It was related to a major solar flare (X17.2/4B), produced in the active region NOAA AR 10486, located slightly east of the central meridian (S16, E08) observed at 10:00 UT. Additionally, a fast CME with a speed $\approx 2500 \text{ km s}^{-1}$ was also observed. The event was well studied, including the corresponding space weather effects and possible SEP acceleration mechanisms (e.g., Gopalswamy et al., 2005; Klassen et al., 2005; Miroshnichenko et al., 2005; Aurass et al., 2006; Li et al., 2007; Waterfall et al., 2023). The global ground-level NM network observed the event onset between 11:05 and 11:15 UT at several NM stations (Figure 1). The strongest count rate increases were observed at MCMD (44.7%), TERA (27.4%), CAPS (18.3%), SOPO (15.2%), and CALG (13.1%) NMs, the detrended data were retrieved from International

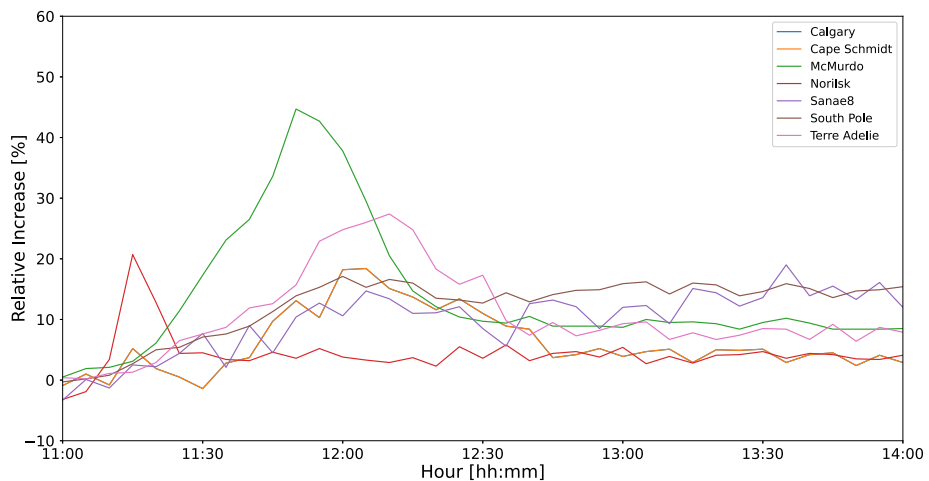


Figure 1 Count rates of selected neutron monitors during GLE #65 on 28 October, 2003. The data are available at <http://gle oulu.fi>.

GLE database <http://gle oulu.fi>. The station standard acronyms and detailed information are given in Table 1.

This event was essentially anisotropic, specifically during the event onset and initial phase. It was also claimed to be observed in solar neutrons (e.g., Chupp and Ryan, 2009), details are given elsewhere (Miroshnichenko et al., 2005), but solar neutrons are not considered in this study. The angular distribution of SEPs was relatively broad, viz. not beam-like (e.g., Bütikofer et al., 2009), because an NM count rate increases consistent in time and amplitude were observed by the bulk of the stations, except for TSMB. We emphasize that this event occurred on the background of significant interplanetary disturbance due to previous eruptions (Grechnev et al., 2014), specifically leading to an interplanetary CME on 26 October, 2003, following the X1.2/3B solar flare, produced by the same active region NOAA AR 10486 (15S, 44E) at 06:17 UT (see the details in Gopalswamy et al., 2005; Miroshnichenko et al., 2005, and references therein). This resulted in a notable fluctuation in the observed NM count rate increases, accordingly leading to non-trivial data analysis.

The GLE #66 (Figure 2) occurred on 29 October, 2003 during one of the strongest geomagnetic storm with the planetary K_p index reaching about 9 (Gopalswamy et al., 2005; Liu and Hayashi, 2006; Gopalswamy et al., 2012). The event also occurred during a deep Forbush decrease, which makes the analysis of this particular GLE specifically challenging, because, on the one hand, it is rather difficult to simulate the particle propagation in a disturbed magnetosphere (e.g., Smart, Shea, and Flückiger, 2000; Bütikofer, 2018), and, on the other hand, the geomagnetic storm led to considerable fluctuations in NM count rates, and finally the Forbush decrease, both interfering with the actual count rate increases due to SEPs.

4. Results of the Analysis

Using the records from the available NM stations during the event(s) (Table 1), and the aforementioned method described in Section 2, we derived the SEP spectra and PADs during

Table 1 Neutron monitors with the corresponding geomagnetic cut-off rigidities and altitudes above the sea level used for the analysis of GLE #65 and #66.

Station	Latitude [deg]	Longitude [deg]	P_c [GV]	Altitude [m]
Alma Aty (AATY)	43.25	76.92	6.67	3340
Apatity (APTY)	67.55	33.33	0.48	177
Athens (ATHN)	37.98	23.78	8.42	260
Baksan (BKSJ)	43.28	42.69	5.6	1700
Barentsburg (BRBJ)	78.03	14.13	0.01	70
Calgary (CALG)	51.08	245.87	1.04	1128
Cape Schmidt (CAPS)	68.92	180.53	0.41	0
Erevan 2 (ERV3)	40.5	44.17	7.58	2000
Erevan 3 (ERV3)	40.5	44.17	7.58	3200
Forth Smith (FSMT)	60.02	248.07	0.25	0
Hermanus (HRMS)	-34.42	19.22	4.90	26
Inuvik (INVK)	68.35	226.28	0.16	21
Irkutsk (IRKT)	52.58	104.02	3.23	435
Irkutsk 2(IRK2)	52.37	100.55	3.23	2000
Irkutsk 3 (IRK3)	51.29	100.55	3.23	3000
Jungfrauojoch (JUN1)	46.55	7.98	4.46	3476
Kerguelen (KERG)	-49.35	70.25	1.01	33
Kiel (KIEL)	54.33	10.13	2.22	54
Lomnický Štit (LMKS)	49.2	20.22	3.72	2634
Magadan (MGDN)	60.12	151.02	1.84	220
McMurdo (MCMD)	-77.85	166.72	0.01	48
Mexico City (MXCO)	19.33	260.8	7.59	2274
Moscow (MOSC)	55.47	37.32	2.13	200
Nain (NAIN)	56.55	298.32	0.28	0
Newark (NWRK)	39.70	284.30	1.97	50
Norilsk (NRLK)	69.26	88.05	0.52	0
Novosibirsk (NVBK)	54.8	83.0	2.33	0
Oulu (OULU)	65.05	25.47	0.69	15
Potchefstroom (PTFM)	-26.7	27.09	6.98	1351
Peawanuck (PWNK)	54.98	274.56	0.16	52
Rome (ROME)	41.9	12.52	6.11	60
Sanae (SNAE)	-71.67	357.15	0.56	856
South Pole (SOPO)	-90.00	0.0	0.01	2820
Terre Adelie (TERA)	-66.67	140.02	0	45
Thule (THUL)	76.60	291.2	0.1	260
Tixie (TXBY)	71.60	128.90	0.53	0
Tsumeb (TSMB)	-19.20	17.58	9.12	1240
Yakutsk (YKTK)	62.03	129.73	1.64	105

GLE #65 and #66 events, aiming to analyse GLEs employing the same method and model, aim inspired by the discussion in Bütikofer and Flückiger (2015).

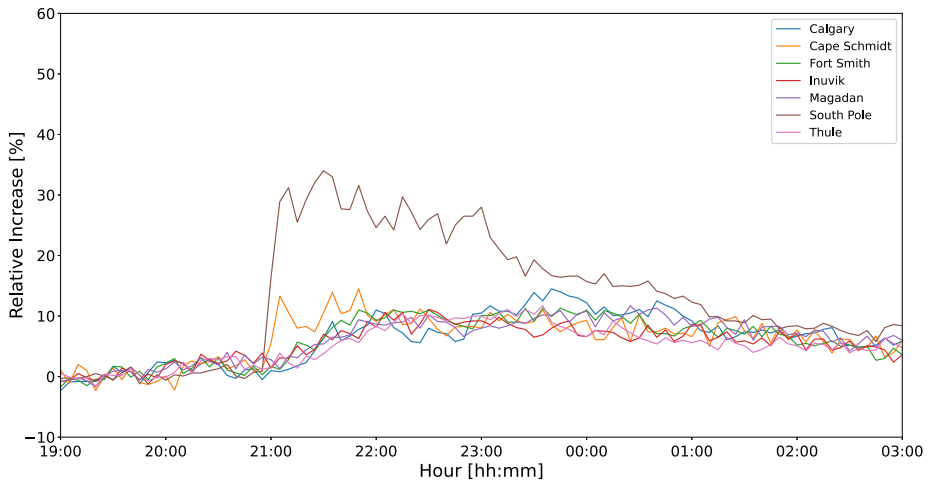


Figure 2 Count rate variation for selected neutron monitors during GLE #66 on 29 October, 2003. The data are available at <http://gle.oulu.fi>.

4.1. Magnetospheric Modelling

Despite the significant interplanetary disturbance, the geomagnetospheric conditions during GLE #65 were relatively quiet with planetary K_p index of about 4. Therefore, the modelling of proton propagation in the geomagnetosphere was straightforward, namely by combining the International Geomagnetic Reference Field (IGRF) geomagnetic model (epoch 2020) as the internal field model (Alken et al., 2021) and the Tsyganenko 89 model as the external field (Tsyganenko, 1989). The employment of the combination of internal and external fields, and using Tsyganenko 89 for the latter, allows straightforward, with the necessary precision, computation of the asymptotic directions and cut-off rigidity of the NMs used in the analysis (Kudela and Usoskin, 2004; Kudela, Bučik, and Bobik, 2008; Nevalainen, Usoskin, and Mishev, 2013). Herein, these computations were performed with MAGNETO-COSMICS code (Desorgher et al., 2005).

Figure 3 shows an illustration of the computed asymptotic directions in the rigidity range 1–5 GV, corresponding to the maximal response, for several NMs used in our analysis. We emphasize that in the analysis we used the 1–20 GV rigidity range, as described in Section 2.

The situation was quite different during GLE #66. This event occurred during a major geomagnetic storm with planetary K_p index of about 9 (e.g., Zurbuchen et al., 2004; Gopalswamy et al., 2005; Pulkkinen et al., 2005; Liu and Hayashi, 2006) and was accompanied by one of the strongest ever observed Forbush decreases (Dorman, Velinov, and Mishev, 2022). The particle propagation in the geomagnetosphere was simulated using a combination of models accounting for the disturbed magnetosphere, that is, IGRF and Tsyganenko 01 (Tsyganenko, 2002) using the new tool OTSO (for details, see Larsen, Mishev, and Usoskin, 2023, and the discussion therein). The Tsyganenko 01 model requires numerous geomagnetic conditions as inputs, these being the dynamic pressure, solar wind speed, Dst index, IMFy, IMFz, G1, and G2 values; with values of 3.2 nPa, 1003 km s⁻¹, 253 nT, 16.4 nT, -19.7 nT, 208.3, and 98.7, respectively, for GLE #66. Note that G1 and G2 are parameters specifically made for the Tsyganenko 01 model that are computed using geomagnetic conditions' data for the hour preceding the event (for details, see Tsyganenko, 2002). Accordingly,

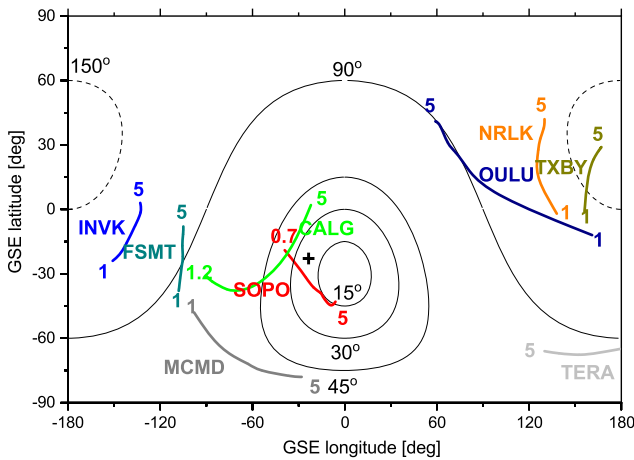
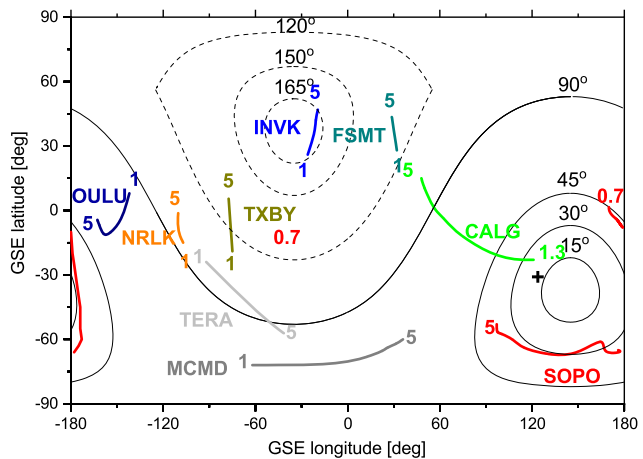


Figure 3 Asymptotic directions in GSE coordinates of several NMs stations during GLE #65 on 28 October, 2003. The asymptotic directions are plotted with NM standard abbreviations and corresponding colour lines in the rigidity range $\sim 1-5$ GV, the exception being SOPO, which is plotted in the rigidity range $\sim 0.7-5$ GV. The cross corresponds to the interplanetary magnetic field direction obtained by the Advanced Composition Explorer (ACE – Smith et al., 1998) space probe. The lines of equal pitch angles relative to the derived anisotropy axis are plotted for 15° , 30° , 45° , and 90° for sunward directions (solid lines), and 150° for anti-Sun direction (dashed lines).

Figure 4 Asymptotic directions during GLE #66 on 29 October, 2003, plotted similarly as for GLE #65.



the asymptotic directions of selected NMs during GLE #66 are presented in Figure 4. We emphasise that the combination of IGRF + Tsyganenko 01 models provides a more realistic modelling of the global NM response and improves the unfolding procedure in the sense of better convergence and smaller residuals as discussed in Larsen, Mishev, and Usoskin (2023).

4.2. Spectra and Anisotropy of SEPs

Using the asymptotic directions computed during the magnetospheric modelling and detrended NM records (see the details in Usoskin et al., 2020b, and references therein) as

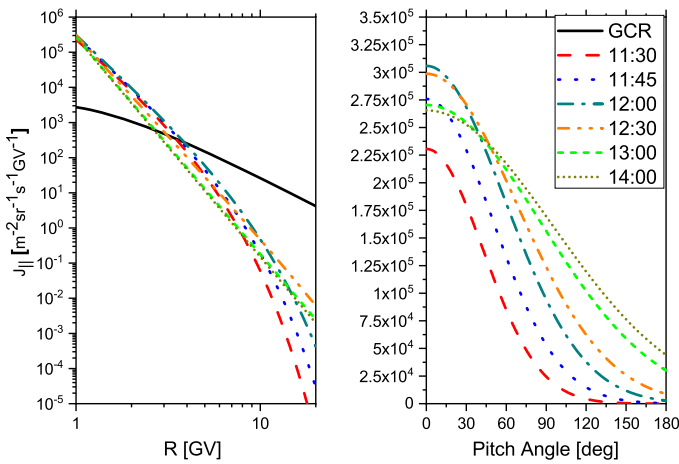


Figure 5 Rigidity spectra (left panel) and PADs (right panel) during GLE #65, the details are given in Table 2. The black solid line denotes the GCR flux, at the time of the event offset. Time (UT) refers to the start of the corresponding five-minute interval over which the data are integrated.

inputs for the method and employing the optimisation itself, we derived the SEP spectra and their PAD during the considered events. The detrended NM records account for short-term GCRs variations, e.g., diurnal variations or recovery phase of Forbush decreases, and allow more realistic and accurate evaluation of the SEP signal in NM records. Therefore, we explicitly accounted the GCR baseline's temporal variability, specifically important during GLE #66 by considering the recovery phase of the deep Forbush decrease during the event; details are given elsewhere (Usoskin et al., 2020b).

Different possible shapes of spectra and angular distribution were examined, namely power-law (modified and simple), exponential, Ellison–Ramaty (Ellison and Ramaty, 1985), Band function (Tylka and Dietrich, 2009), and single or double Gaussian, respectively, for the PAD. In case of similar quality of the fit, we gave preference to the simplest model.

The best fit of the SEP spectra during GLE #65 is obtained with a modified power-law rigidity spectrum, that is, the proton flux $J_{||}(P)$, where P is rigidity in GV, is described with

$$J_{||}(P) = J_0 P^{-(\gamma + \delta\gamma(P-1))}, \quad (3)$$

where the SEPs are with rigidity $P > 1$ GV, arriving along the axis of symmetry determined by geographic latitude Ψ and longitude Λ , γ is the spectral index, and $\delta\gamma$ represent the spectrum steepening. For SEPs with $P \leq 1$ GV, the rigidity spectrum is approximated as

$$J_{||}(P) = J_0 P^{-(\gamma + \delta\gamma \cdot P)}. \quad (4)$$

For PAD, the best fit is achieved using a single Gaussian,

$$G(\alpha(P)) \sim \exp(-\alpha^2/\sigma^2), \quad (5)$$

where α is the pitch angle, and σ accounts for the width of the distribution.

Figure 5 provides an illustration of several SEP spectra during the initial and main phase of the event (roughly corresponding to the prompt component and early stage of delayed component of the GLE particles (Vashenyuk et al., 2006; Mishev et al., 2022)), while the full details are given in Table 2.

Table 2 Derived spectral and angular characteristics of SEPs during GLE #65 on 28 October, 2003 fitted with the modified power-law rigidity spectrum (Equation 3). The columns depict the integration interval (1), particle flux at 1 GV (2), spectrum slope (3), steepening of the spectrum (4), width of the angular distribution (5), anisotropy axis position in GEO coordinates (6,7), merit function \mathcal{D} (8), and normalised to degrees of freedom χ_r^2 (9).

Integration interval UT	J_0 [$\text{m}^{-2} \text{s}^{-1} \text{sr}^{-1} \text{GV}^{-1}$]	γ	$\delta\gamma$ [GV^{-1}]	σ^2 [rad^2]	Ψ [degrees]	Λ [degrees]	\mathcal{D} [%]	χ_r^2
11:15 – 11:20	1.22E5	4.61	0.45	1.1	−49.0	−155.0	17.2	1.3
11:20 – 11:25	1.35E5	4.65	0.4	1.1	−49.0	−155.0	15.1	1.2
11:25 – 11:30	1.52E5	4.68	0.38	1.3	−48.0	−157.0	12.2	1.02
11:30 – 11:35	1.981E5	4.72	0.31	1.45	−42.0	−160.0	11.2	1.02
11:35 – 11:40	2.17E5	4.75	0.28	1.52	−49.0	−165.0	10.1	1.02
11:40 – 11:45	2.387E5	4.79	0.26	1.55	−66.0	−170.0	9.0	1.01
11:45 – 11:50	2.81E5	4.8	0.25	1.7	−63.0	−172.0	8.9	1.01
11:50 – 11:55	3.284E5	4.81	0.25	1.8	−60.0	−174.0	8.8	1.01
11:55 – 12:00	3.188E5	4.85	0.25	1.95	−62.0	−172.0	9.2	1.02
12:00 – 12:05	3.008E5	4.96	0.22	2.1	−63.0	−160.0	8.2	1.01
12:05 – 12:10	3.0E5	5.23	0.2	2.5	−52.0	−165.0	8.5	1.02
12:10 – 12:15	2.95E5	5.35	0.18	2.57	−48.0	−160.0	8.7	1.01
12:15 – 12:20	2.932E5	5.53	0.17	2.55	−45.0	−164.0	9.0	1.02
12:20 – 12:25	2.96E5	5.65	0.1	2.7	−35.0	−172.0	8.0	1.05
12:25 – 12:30	2.981E5	5.73	0.03	2.85	−28.0	−170.0	6.5	1.01
12:30 – 12:35	2.987E5	5.7	0.02	2.8	−25.0	−172.0	7.8	1.1
12:35 – 12:40	2.952E5	5.74	0.02	2.9	−30.0	−174.0	7.5	1.05
12:40 – 12:45	2.913E5	5.83	0.01	3.2	−28.0	−176.0	7.1	1.03
12:45 – 12:50	2.841E5	5.95	0.01	3.8	−27.0	−179.0	6.1	1.01
12:50 – 12:55	2.875E5	6.0	0.0	4.1	−32.0	−179.0	6.7	1.1
12:55 – 13:00	2.804E5	5.9	0.0	4.3	−32.0	−177.0	6.0	1.0
13:00 – 13:05	2.704E5	6.18	0.0	4.5	−31.0	−170.0	5.6	0.99
13:05 – 13:10	2.684E5	6.18	0.0	4.5	−28.0	−175.0	5.6	1.0
13:10 – 13:15	2.695E5	6.2	0.0	4.52	−30.0	−179.0	5.7	0.99
13:15 – 13:20	2.712E5	6.2	0.0	4.55	−33.0	−179.0	5.8	0.99
13:20 – 13:25	2.683E5	6.2	0.0	4.55	−34.0	−178.0	6.1	0.99
13:25 – 13:30	2.694E5	6.2	0.0	4.55	−36.0	−179.0	6.2	0.97
13:30 – 13:35	2.724E5	6.22	0.0	4.57	−35.0	−177.0	5.0	0.98
13:35 – 13:40	2.71E5	6.22	0.0	4.7	−34.0	−177.0	5.1	0.98
13:40 – 13:45	2.705E5	6.23	0.0	4.9	−37.0	−175.0	6.5	1.01
13:45 – 13:50	2.7E5	6.23	0.0	5.1	−38.0	−178.0	5.5	1.0
13:50 – 13:55	2.684E5	6.23	0.0	5.2	−38.0	−175.0	5.5	0.99
13:55 – 14:00	2.672E5	6.24	0.0	5.3	−40.0	−177.0	5.7	0.99
14:00 – 14:05	2.655E5	6.25	0.0	5.5	−39.0	−175.0	5.6	1.0
14:05 – 14:10	2.65E5	6.26	0.0	5.5	−35.0	−176.0	5.7	0.99
14:10 – 14:15	2.64E5	6.27	0.0	5.6	−36.0	−177.0	5.6	0.98
14:15 – 14:20	2.63E5	6.27	0.0	5.6	−37.0	−178.0	5.8	0.99
14:20 – 14:25	2.61E5	6.28	0.0	5.65	−34.0	−177.0	5.7	0.99
14:25 – 14:30	2.6E5	6.3	0.0	5.7	−36.0	−178.0	5.8	0.98

Table 2 (Continued)

Integration interval UT	J_0 [$\text{m}^{-2} \text{s}^{-1} \text{sr}^{-1} \text{GV}^{-1}$]	γ	$\delta\gamma$ [GV^{-1}]	σ^2 [rad^2]	Ψ [degrees]	Λ [degrees]	\mathcal{D} [%]	χ_r^2
14:30–14:35	2.58E5	6.3	0.0	5.7	−35.0	−179.0	5.7	0.99
14:35–14:40	2.57E5	6.32	0.0	5.8	−34.0	−179.0	5.8	0.98
14:40–14:45	2.55E5	6.33	0.0	5.8	−33.0	−179.0	5.5	0.99
14:45–14:50	2.54E5	6.33	0.0	5.9	−37.0	−179.0	5.8	0.98
14:50–14:55	2.53E5	6.35	0.0	5.9	−36.0	−178.0	5.9	0.98
14:55–15:00	2.52E5	6.37	0.0	6.0	−36.0	−179.0	5.9	1.01
15:00–15:05	2.51E5	6.4	0.0	6.1	−35.0	−177.0	5.5	0.99
15:15–15:20	2.5E5	6.42	0.0	6.3	−34.0	−177.0	5.7	0.98
15:30–15:35	2.495E5	6.44	0.0	6.5	−35.0	−178.0	5.7	0.99
15:45–15:50	2.49E5	6.47	0.0	6.7	−36.0	−179.0	5.8	1.01
16:00–16:05	2.48E5	6.5	0.0	7.1	−38.0	−179.0	6.2	1.03
16:30–16:35	2.47E5	6.5	0.0	7.2	−34.0	−177.0	6.2	1.04
17:00–17:05	2.46E5	6.55	0.0	7.4	−38.0	−179.0	6.5	1.03
17:30–17:35	2.43E5	6.57	0.0	8.1	−31.0	−177.0	6.5	1.01
18:00–18:05	2.4E5	6.6	0.0	8.4	−40.0	−179.0	6.6	1.03
18:30–18:35	2.38E5	6.7	0.0	8.6	−33.0	−179.0	6.7	1.02
19:00–19:05	2.35E5	6.8	0.0	8.8	−32.0	−179.0	6.9	1.04
20:00–20:05	2.01E5	6.9	0.0	9.2	−33.0	−178.0	8.0	1.05
21:00–21:05	2.0E5	7.0	0.0	9.5	−35.0	179.0	8.5	1.06
22:00–22:05	1.85E5	7.1	0.0	9.8	−33.0	179.0	7.8	1.03
23:00–23:05	1.83E5	7.2	0.0	10.1	−34.0	178.0	8.5	1.06
(+1)00:00–00:05	1.62E5	7.3	0.0	12.0	−35.0	177.0	9.0	1.05
(+1)01:00–01:05	1.58E5	7.3	0.0	13.0	−37.0	175.0	11.0	1.07
(+1)02:00–02:05	1.52E5	7.3	0.0	14.0	−41.0	174.0	12.0	1.08
(+1)03:00–03:05	1.47E5	7.3	0.0	15.0	−42.0	175.0	10.0	1.06
(+1)04:00–04:05	1.41E5	7.4	0.0	16.0	−45.0	171.0	9.0	1.05

The derived SEP spectra were moderately hard during the initial (11:15–11:45 UT) and main (11:45–12:30 UT) phases of the event. The SEP flux slowly rose to the peak value, (11:50 UT), and afterwards gradually decreased throughout the event. The SEP spectra were moderately steep, that is, without a notable roll-off, which vanished in the late phase of the event after 12:50 UT. Hence, after the main phase of the event, the SEP spectra were soft, described with pure power-law rigidity spectra and revealing a decrease in the particle flux compared to the initial stages. The derived angular distribution gradually broadened throughout the event.

The fit with the exponential spectrum, often used for prompt component description (e.g., Vashenyuk et al., 2006), viz.

$$J_{\parallel}(P) = J_0 \exp(-P/P_0), \quad (6)$$

where $J_{\parallel}(P)$ is defined in the same way as in Equation 4, while P_0 is a characteristic proton rigidity, was found unable to describe the rigidity/energy distribution of SEPs. The exponential spectrum produced a satisfactory fit only for low-rigidity cut-off high-altitude NMs

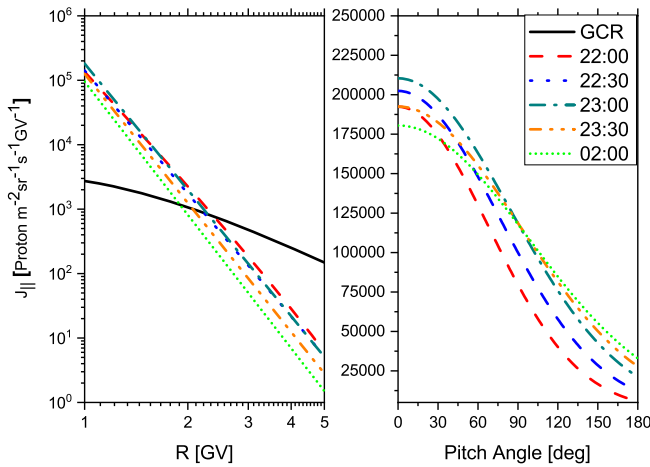


Figure 6 Rigidity spectra (left panel) and PADs (right panel) of SEPs reconstructed here for GLE #66, the details are given in Table 3.

such as CALG and SOPO, but not for the sea-level stations, implying for a moderate roll-off of the spectrum. In contrast to Miroschnichenko et al. (2005), the results of our analysis do not favour double-Gaussian PAD, that is, Sun + anti-Sun particle arriving direction(s), and yield a single Gaussian PAD. We emphasize that according to our analysis, the Sun – anti-Sun PAD can describe the experimental data only for a short period at the initial phase of the event with the value of B (the contribution of anti-Sun arriving particles, see Equation 7) of $\approx 0.1 - 0.15$ with the corresponding decrease of J_0 , whilst for the main and late phases of the event, the D and χ_r^2 greatly increased to ≈ 25 and ≈ 1.8 , respectively. For illustration, the double Gaussian PAD (Sun–anti-Sun) is given by

$$G(\alpha(P)) \approx \exp(-\alpha^2/\sigma_1^2) + B \exp(-(\alpha - \pi)^2/\sigma_2^2), \tag{7}$$

where α is the pitch angle, σ_1 and σ_2 are parameters governing the width of the distribution, and B accounts for the contribution of the particles arriving from the anti-Sun direction.

A similar analysis was performed for GLE #66 using detrended NM records, with the deep Forbush decrease and its recovery in GCR fluxes being explicitly considered during the analysis (Usoskin et al., 2020b). The event was also fitted with modified power-law spectra and single Gaussian PAD, as illustrated in Figure 6, with the details given in Table 3. The analysis of this event was rather challenging because it occurred during a significant magnetospheric disturbance and a deep Forbush decrease, resulting in large fluctuations of the observed NM count rates leading to not straightforward modelling, specifically of the asymptotic directions of the stations.

The derived SEP rigidity spectrum was found softer during GLE #66 than that during GLE #65. The SEP flux rose rapidly, but was not impulse-like, within a similar time span, that is, the flux started to rise after the event onset at 21:00 UT till 21:30 UT, afterwards gradually decreased. Similarly to the previous event (GLE #65), we derived gradual softening of the SEP spectrum throughout the event, with marginal steepening of the spectrum $\delta\gamma$, which vanished after 22:15 UT, that is, the rigidity spectra were nearly a pure power law during the late phase of the event. The derived PAD broadened out similarly to the previous event.

Table 3 Derived spectral and angular characteristics of SEPs during GLE #66 on 29 October, 2003 fitted with the modified power-law rigidity spectrum. The notations are the same as in Table 2.

Integration interval UT	J_0 [$\text{m}^{-2} \text{s}^{-1} \text{sr}^{-1} \text{GV}^{-1}$]	γ	$\delta\gamma$ [GV^{-1}]	σ^2 [rad^2]	Ψ [degrees]	Λ [degrees]	\mathcal{D} [%]	χ_r^2
21:00–21:05	6.57E4	4.81	0.35	0.9	−33.0	25.0	10.0	1.2
21:05–21:10	7.24E4	4.82	0.35	0.91	−31.0	22.0	11.0	1.2
21:10–21:15	7.87E4	4.83	0.34	0.92	−30.0	20.0	12.0	1.2
21:15–21:20	8.57E4	4.85	0.32	0.95	−27.0	17.0	11.0	1.1
21:20–21:25	1.083E5	5.1	0.3	1.1	−28.0	12.0	10.0	1.1
21:25–21:30	1.384E5	5.44	0.28	1.25	−30.0	14.0	10.5	1.1
21:30–21:35	1.522E5	5.57	0.25	1.77	−32.0	12.0	9.9	0.95
21:35–21:40	1.4734E5	5.62	0.2	2.01	−29.0	9.0	10.2	1.05
21:40–21:45	1.431E5	5.69	0.18	2.28	−31.0	7.0	10.1	1.1
21:45–21:50	1.383E5	5.77	0.15	2.52	−32.0	3.0	9.8	1.03
21:50–21:55	1.375E5	5.79	0.14	2.72	−28.0	3.0	9.7	1.05
21:55–22:00	1.364E5	5.8	0.12	2.93	−25.0	4.0	9.8	1.04
22:00–22:05	1.352E5	5.81	0.1	3.73	−21.0	4.0	8.2	1.03
22:05–22:10	1.364E5	5.85	0.09	4.8	−25.0	10.0	8.3	1.02
22:10–22:15	1.375E5	5.9	0.05	5.9	−30.0	17.0	8.0	1.02
22:15–22:20	1.381E5	6.0	0.05	7.75	−35.0	15.0	7.9	1.03
22:20–22:25	1.392E5	6.11	0.0	8.5	−33.0	20.0	8.2	1.01
22:25–22:30	1.4E5	6.22	0.0	9.1	−35.0	24.0	8.1	1.02
22:30–22:35	1.412E5	6.34	0.0	10.5	−40.0	25.0	8.2	1.01
22:35–22:40	1.385E5	6.35	0.0	12.0	−41.0	24.0	8.3	1.02
22:40–22:45	1.347E5	6.36	0.0	14.0	−40.0	22.0	8.2	1.02
22:45–22:50	1.33E5	6.36	0.0	15.0	−42.0	23.0	8.1	1.01
22:50–22:55	1.55E5	6.43	0.0	15.0	−40.0	25.0	8.0	1.05
22:55–23:00	1.78E5	6.48	0.0	15.0	−37.0	24.0	9.0	0.99
23:00–23:05	1.813E5	6.51	0.0	16.0	−39.0	26.0	7.0	0.99
23:05–23:10	1.685E5	6.53	0.0	16.0	−37.0	24.0	7.0	0.99
23:10–23:15	1.53E5	6.53	0.0	17.0	−36.0	22.0	8.0	0.98
23:15–23:20	1.41E5	6.55	0.0	18.0	−38.0	22.0	6.7	0.96
23:20–23:25	1.378E5	6.61	0.0	18.0	−35.0	18.0	8.4	1.05
23:25–23:30	1.33E5	6.63	0.0	18.0	−34.0	20.0	9.2	1.1
23:30–23:35	1.253E5	6.65	0.0	18.0	−37.0	21.0	9.7	1.1
23:35–23:40	1.241E5	6.66	0.0	19.0	−33.0	22.0	10.0	1.2
23:40–23:45	1.23E5	6.67	0.0	19.0	−34.0	21.0	10.0	1.2
23:45–23:50	1.21E5	6.68	0.0	20.0	−37.0	25.0	10.0	1.2
23:50–23:55	1.25E5	6.63	0.0	21.0	−39.0	28.0	9.0	1.1
23:55–00:00	1.28E5	6.55	0.0	21.0	−41.0	29.0	9.0	0.9
(+1)00:00–00:05	1.33E5	6.5	0.0	21.0	−39.0	29.0	8.0	0.95
(+1)00:05–00:10	1.325E5	6.5	0.0	21.0	−35.0	20.0	8.0	0.95
(+1)00:10–00:15	1.321E5	6.51	0.0	22.0	−28.0	18.0	9.0	0.97
(+1)00:15–00:20	1.31E5	6.52	0.0	22.0	−32.0	15.0	9.0	1.05
(+1)00:20–00:25	1.31E5	6.52	0.0	22.0	−28.0	10.0	10.0	1.07

Table 3 (Continued)

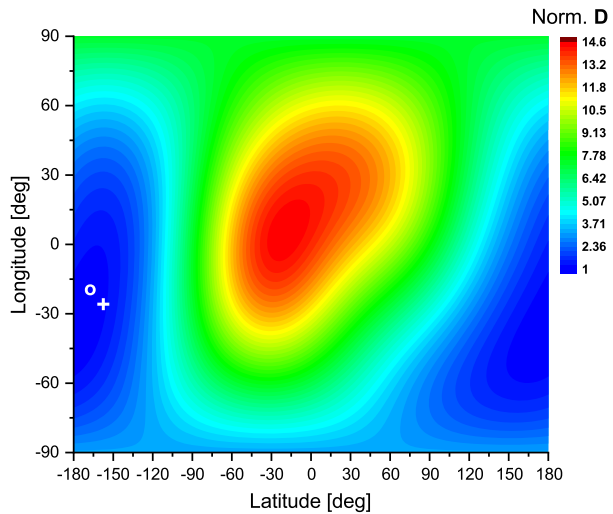
Integration interval UT	J_0 [$\text{m}^{-2} \text{s}^{-1} \text{sr}^{-1} \text{GV}^{-1}$]	γ	$\delta\gamma$ [GV^{-1}]	σ^2 [rad^2]	Ψ [degrees]	Λ [degrees]	\mathcal{D} [%]	χ_r^2
(+1)00:25–00:30	1.3E5	6.53	0.0	22.0	–15.0	7.0	9.0	1.1
(+1)00:30–00:35	1.3E5	6.55	0.0	23.0	–18.0	8.0	10.0	1.1
(+1)00:35–00:40	1.297E5	6.55	0.0	23.0	–12.0	5.0	10.0	1.2
(+1)00:40–00:45	1.295E5	6.57	0.0	23.0	–10.0	5.0	9.0	1.1
(+1)00:45–00:50	1.29E5	6.57	0.0	24.0	–8.0	0.0	10.0	1.1
(+1)00:50–00:55	1.286E5	6.59	0.0	24.0	–12.0	–1.0	10.0	1.1
(+1)00:55–01:00	1.283E5	6.6	0.0	24.0	–7.0	–2.0	11.0	1.2
(+1)01:00–01:05	1.26E5	6.6	0.0	25.0	–5.0	–2.0	8.0	0.95
(+1)01:05–01:10	1.243E5	6.61	0.0	25.0	–4.0	–3.0	13.0	1.2
(+1)01:10–01:15	1.21E5	6.62	0.0	25.0	–5.0	–5.0	12.0	1.1
(+1)01:15–01:20	1.175E5	6.62	0.0	25.0	–7.0	–8.0	10.0	1.2
(+1)01:20–01:25	1.15E5	6.64	0.0	25.0	–3.0	–5.0	11.0	1.1
(+1)01:25–01:30	1.142E5	6.65	0.0	25.0	–2.0	–8.0	12.0	1.2
(+1)01:30–01:35	1.113E5	6.7	0.0	25.0	–7.0	–10.0	12.0	1.1
(+1)01:35–01:40	1.114E5	6.75	0.0	25.0	–5.0	–15.0	11.0	1.2
(+1)01:40–01:45	1.082E5	6.77	0.0	25.0	–8.0	–15.0	11.0	1.2
(+1)01:45–01:50	1.051E5	6.79	0.0	26.0	–3.0	–20.0	12.0	1.2
(+1)01:50–01:55	1.01E5	6.83	0.0	25.0	–10.0	–20.0	12.0	1.3
(+1)01:55–02:00	9.85E4	6.85	0.0	25.0	–8.0	–20.0	13.0	1.3
(+1)02:00–02:05	9.5E4	6.87	0.0	26.0	–3.0	–25.0	15.0	1.4

4.3. Confidence Limits and Fit Quality

An important issue during optimisation procedures is the existence, uniqueness, and stability of the derived solution(s), i.e., the existence of a global minimum of the fitting function and related robustness of the method (Engl, Hanke, and Neubauer, 1996; Strutz, 2011). We note that the convergence of the solution can be unstable against small variations of the input data (e.g., fluctuations of the recorded NM count rates) and the initial guess because the inverse problems are typically ill-conditioned and/or ill-posed (e.g., Strutz, 2011). Besides, non-linear ill-posed inverse problems often converge to a minimum, which can be local, leading to multiple possible solutions (Dennis and Schnabel, 1996; Aster, Borchers, and Thurber, 2005). Herein, such situations can arise from the large fluctuations of NM response between different stations (data points) and possible employment of inappropriate regularisation factors, specifically during the initial iterations (More, Garbow, and Hillstrom, 1980; Tikhonov et al., 1995).

In our study, an application of unfolding algorithms with variable regularisation (e.g., Aleksandrov, 1971; Tikhonov et al., 1995; Mishev, Mavrodiev, and Stamenov, 2005; Huber, 2019) and forward modelling similarly to Cramp et al. (1997), Mishev et al. (2022) were applied. The latter is specifically important in order to derive properly the apparent source position to which the final fit is very sensitive (Bütikofer and Flückiger, 2015). In this way, we constrained the model parameters space and eventually obtained a robust solution, employing the aforementioned fit criteria (Schuster et al., 2012; Huber, 2019). This approach allowed the acquisition of practically the same set of model best-fit parameters within the

Figure 7 Contour plot of normalised to minimum \mathcal{D} (see Table 2) for the best-fit solutions as a function of the geographical coordinates of the apparent source position during GLE #65 event on 28 October, 2003 at 12:30 UT. The small white oval corresponds to the derived apparent source position, while the white cross corresponds to the observed IMF direction based on ACE space probe measurements.



corresponding uncertainties when slightly varying the initial guess. Figure 7 illustrates the result of forward modelling as a contour plot of the merit function \mathcal{D} for the best-fit solutions as the function of geographic coordinates for GLE #65. Hence, the large number of NM stations with different responses and the computed contour plots of \mathcal{D} for the best-fit solutions allowed us to assure the uniqueness and stability of the latter, that is the reconstructed SEP characteristics. We note that when the initial guess was far from the final minimum, that is the minimum corresponding to a solution of the inverse problem (reconstructed spectrum), the derived solution possessed significantly greater residual compared to that in Table 2 or was not physical, e.g., wider than 2π PAD.

A comparison between the modelled and experimental responses of selected NMs over the event is presented in Figure 8. The quality of the unfolding is similar for the bulk of NMs used in the analysis, except for CALG and FSMT where an apparent difference between modelled and experimental responses is observed, specifically during the late phase of the event. We note that a wider PAD distribution can improve the observed difference for CALG and FSMT, both with asymptotic directions looking in anti-Sun direction of SEP flux, but would violate the uniformity of residuals distribution, which is one of the fit criteria. Therefore, we preferred to keep the derived fit, despite the not-very-precise description of the FSMT station response.

The derived SEP flux J_0 is shown, along with the 95% confidence interval, in Figure 9 for different phases of GLE #65. We note that the accuracy of the apparent source position assessment was about $5^\circ - 8^\circ$ and about 10% for the spectral slope. The isotropisation of the particle flux during the late phase of the event, after 16:00 UT, resulted in slightly greater residuals and, therefore, smaller precision of the estimation of the spectral and angular characteristics.

Similar computations were performed for the analysis of GLE #66 with the result of forward modelling presented in Figure 10 and the comparison between the modelled and measured responses of selected NMs in Figure 11. Accordingly, the derived best-fit SEP flux along with the 95% confidence levels are shown in Figure 12.

We note that the analysis of GLE #66 was more complicated, due to complex geomagnetospheric conditions, the Forbush decrease and large fluctuations of the NM count rates between the stations, leading to greater residuals than those for GLE #65 (see, e.g., the dif-

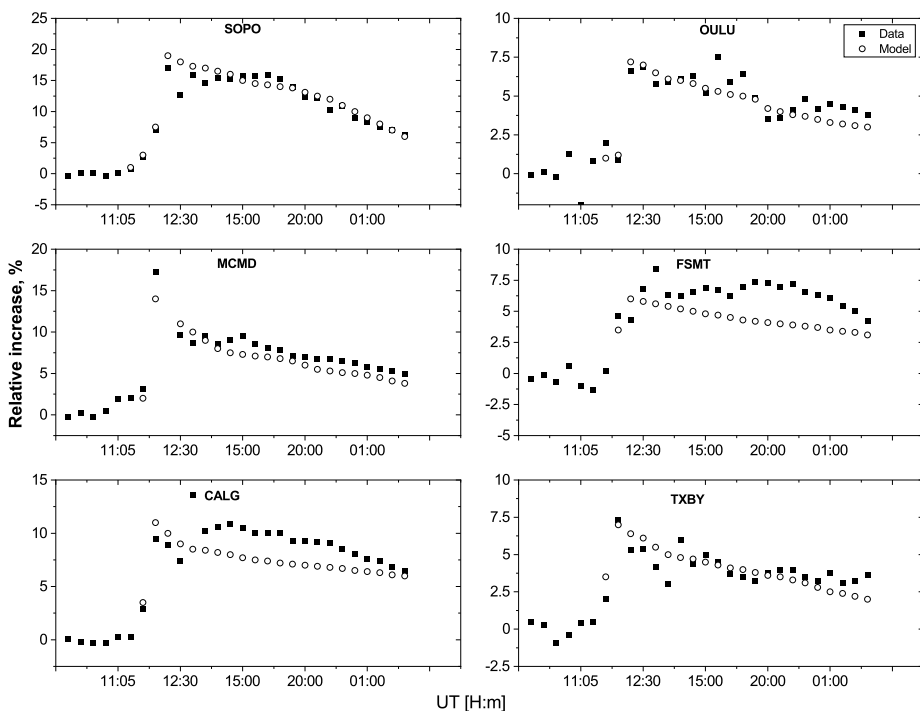
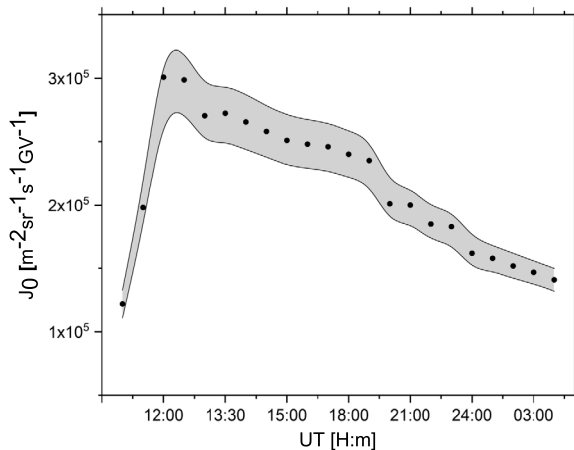


Figure 8 Modelled and measured count rate increases of selected NMs during GLE #65.

Figure 9 The best-fit values of SEP flux J_0 (dots – see Table 2) along with the 95% confidence intervals (grey shading) during different phases of GLE #65.



ference between the modelled and experimental responses of CALG, INVK, and OULU) and accordingly to poorer accuracy of reconstructed spectral characteristics, with yet satisfactory results achieved.

Figure 10 Contour plot of minimum \mathcal{D} (see Table 3) for the best-fit solutions as a function of the geographic coordinates of the apparent source position for GLE #66 event on 29 October, 2003 at 21:30 UT, normalised to the minimal \mathcal{D} . The small white oval and cross correspond to the derived apparent source position and the IMF direction derived from the ACE space-probe data, respectively.

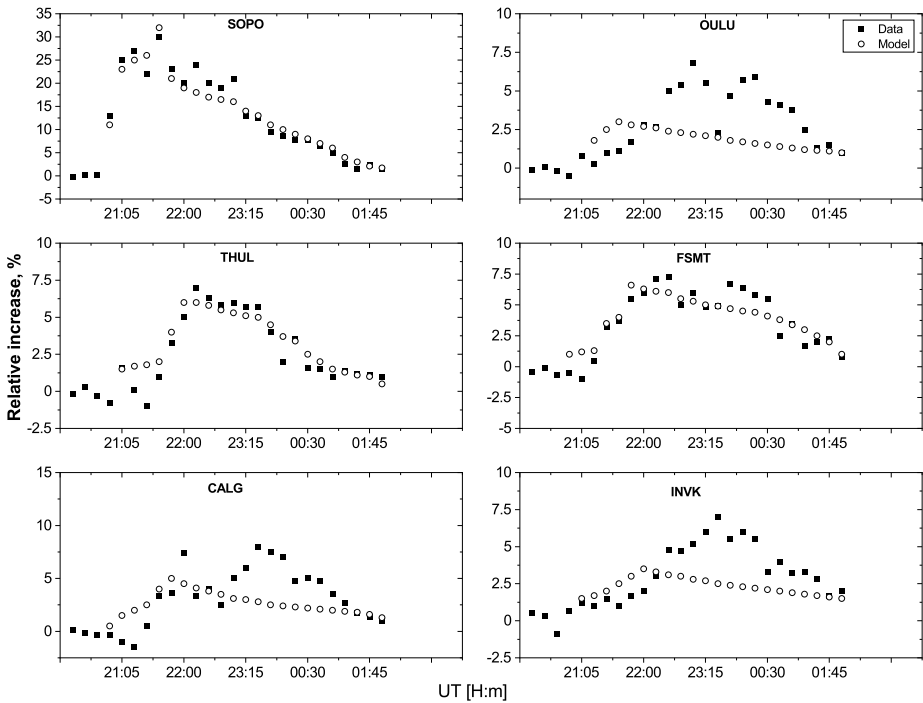
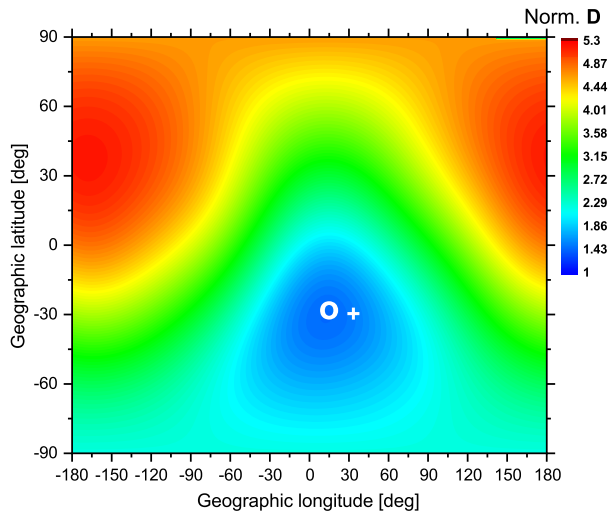


Figure 11 Modelled and observed count rate increases of selected NMs during GLE #66.

4.4. Particle Fluence

We also calculated the event-integrated flux (fluence) of SEP particles during GLEs #65 and #66 using the data from Tables 2–3, integrating it over the obtained energy and PAD dependencies and the corresponding time intervals. Results of the calculation are shown in

Figure 12 Similar to Figure 9 but for GLE #66. The values are given in Table 3.

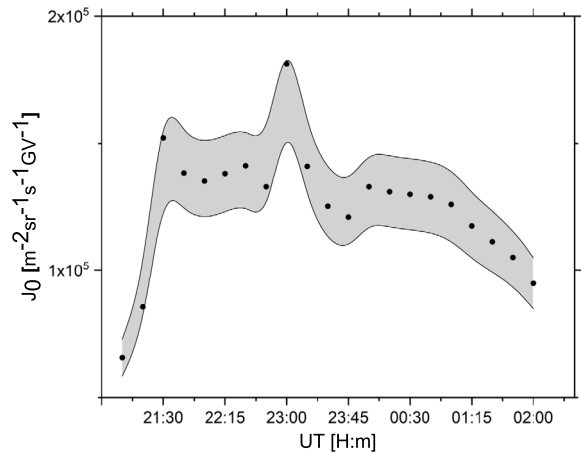


Figure 13 Fluence of SEPs for GLE events #65 and #66. The results of this work are shown in blue and orange. Reconstructions made using the ‘effective energy’ method (see text for details) are shown in green and red. For both methods, 1σ uncertainties of the fluence reconstruction are plotted with semitransparent colour.

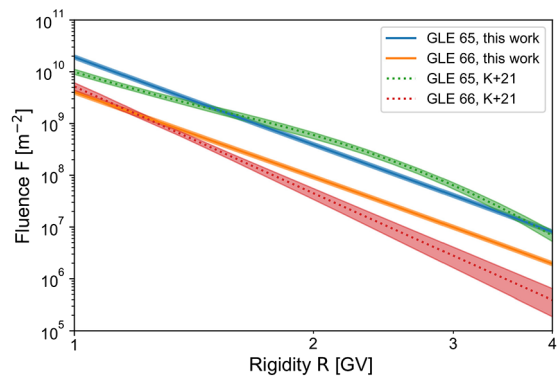


Figure 13 together with results of an independent method of the fluence estimate (Koldobskiy, Kovaltsov, and Usoskin, 2018; Koldobskiy et al., 2019b; Usoskin et al., 2020a), which considers every NM as a proportional counter, whose SEP-related count rate is directly proportional to the fluence of SEP particles with energy above the ‘effective’ energy E_{eff} , where E_{eff} and the coefficient of proportionality are (quasi)constant for a given NM. Figure 13 shows the results of the best-fit of fluence points reconstructed with this method parameterized by the modified Band function (Koldobskiy et al., 2021). Overall, the results from both methods are in satisfactory agreement with a small discrepancy for the high-energy part of GLE #66, due to the apparent difference between the modified power-law and Band functions and anisotropy effects.

5. Discussion and Conclusions

In this paper, we present the results of a detailed analysis of the first two GLEs of the Halloween 2003 series, which are GLE #65 on 28 October, 2003 and GLE #66 on 29 October, 2003. We reconstructed the spectra and angular distribution of GLE-causing SEPs, including their dynamical evolutions in the course of the event, with unprecedented time resolution and accuracy. Among all the studied possibilities for SEP spectra, the best fit was obtained

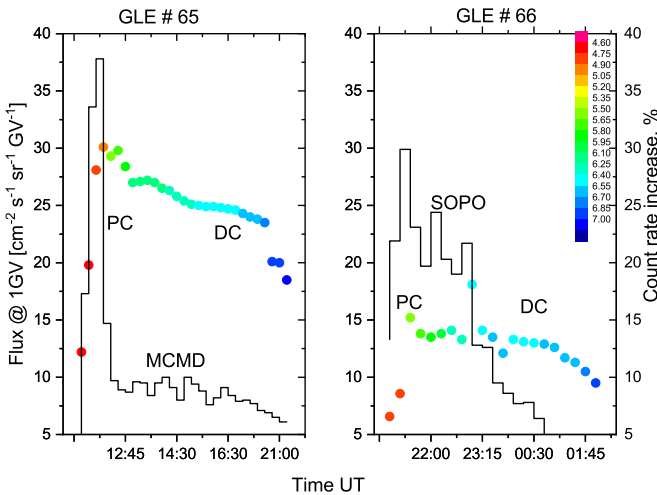


Figure 14 SEP flux at 1 GV, spectral slope evolution for the prompt (PC) and delayed (DC) components as denoted in the colour map and variation (black line) of MCMD and SOPO count rate increases during GLE #65 for the former and GLE #66 for the latter.

using a modified power-law rigidity spectrum and Gauss-like angular distribution for both events. The SEP spectrum during both events softened gradually along with the anisotropy decreasing in the course of the events.

However, despite being produced by subsequent eruptions in the same active region, the GLEs #65 and #66 were not morphologically identical (see Figure 14), in the sense of the SEP flux J_0 at 1 GV, the spectral slope evolution and the NM count rate increase of stations revealing the maximum. During GLE #65, count rates of MCMD NM clearly depicted both the prompt component (PC) of the SEP event, viz. the initial sharp rise accompanied by the hard spectrum and increase of the SEP flux, and the delayed component (DC) when both a gradual decrease of the SEP flux and softening of the spectrum were observed. According to Vashenyuk et al. (2006), most of the GLEs exhibit hard spectra at low rigidities, which tend to be steeper at greater ones, accompanied by an anisotropic angular distribution as typical for a PC. The second, delayed component became dominant after about 1–2 hours after the event onset, revealing softer spectrum, and with nearly isotropic angular distribution.

The situation was different for GLE #66. In this case, the counts of the SOPO NM can not be straightforwardly disentangled into the PC and DC. We note that MCMD and SOPO were the stations with the maximal count rate increase during GLEs #65 and #66, respectively.

The latter observation can be explained by interplanetary transport effects. For example, SEPs can be broadly distributed in the heliosphere due to some additional ones to the focused transport processes such as diffusion, which can take effect in the vicinity of the Sun or in the interplanetary space (e.g., Desai and Giacalone, 2016; van den Berg, Strauss, and Effenberger, 2020, and the discussion therein). Besides, sudden changes in the IMF direction can decouple accelerated solar ions from the magnetic field lines, thus a cross-field transport can be effective (for details, see Kocharov et al., 2020, and the discussion therein). Although SEPs propagate in the interplanetary space mostly along the IMF lines, enhanced solar-wind turbulence can play an important role in particle scattering and transport across the average magnetic field, including perpendicular transport (e.g., Laitinen and Dalla, 2017; Laitinen et al., 2023) and drifts (Dalla et al., 2013). Significant fluctuations in the IMF direction observed by the ACE space probe imply major disturbance and the related geomagnetic

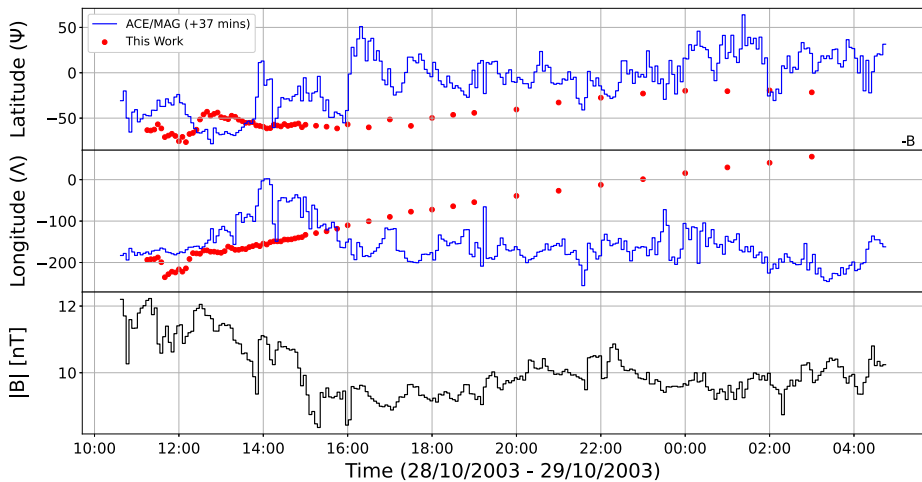


Figure 15 (Top and middle) Latitude and longitude of IMF in GSE coordinates according to the ACE measurements (blue line) and the coordinates of the apparent arrival direction of proton flux derived here (red dots) for GLE #65. (Bottom) The interplanetary magnetic field data corrected for the transit time between the L1 location and the Earth considering the measured solar wind speed according to SOHO/CELIAS (Hovestadt et al., 1995).

storm, and can explain the observations and the deduced SEP properties during GLE #66. Therefore in this case, a full detailed model of the complicated interplanetary transport of SEPs is necessary (e.g., Waterfall et al., 2022), which is beyond the scope of this study considering SEP in the vicinity of Earth.

On the other hand, the derived arrival direction of SEPs during GLE #65 appears close to the observed IMF direction. This is specifically seen for the prompt component, for details see the top and middle panels of Figure 15 and Table 2. We note that during this event the PC was extended (e.g., Kocharov et al., 2023, and the discussion therein), implying prolonged acceleration processes. However, an apparent difference between the arrival direction and the observed IMF is presented during the delayed component, particularly in longitude. This suggests a possible additional diffusion of GLE particles during their propagation in the interplanetary space as discussed above, and can explain the difference between the modelled and observed responses of stations CALG and FSMT with the anti-Sun viewing direction. Besides, as seen in the bottom panel of Figure 15, abrupt changes in the magnetic field magnitude were observed by the ACE/MAG instrument, which may support the idea of the cross-field transport of high-energy protons.

A similar analysis was performed for GLE #66, for details see Figure 16. In this case, there was almost a coincidence between ACE measurements and the latitude of the derived arrival of GLE particles throughout the whole event, yet an apparent difference in the longitude was revealed. Considering the magnetospheric disturbance and the possible complicated interplanetary transport of SEPs, one can understand the difference between the modelled and experimental responses of several NMs during GLE #66.

During the onset and initial phases, viz. PC, of both events, the rigidity spectra were moderately hard $\gamma \approx 4.6\text{--}5.5$ with notable steepness $\delta\gamma \approx 0.3\text{--}0.4$ [GV^{-1}]. The angular distributions of SEPs were relatively narrow with $\sigma^2 \approx 1.1\text{--}1.5$ and $\approx 0.9\text{--}1.3$ [rad^2] for GLEs #65 and #66, respectively. At later stages (DC) of the events, the SEP flux gradually decreased with the steepness of the spectra vanishing, that is $\delta\gamma = 0$, implying a pure power-

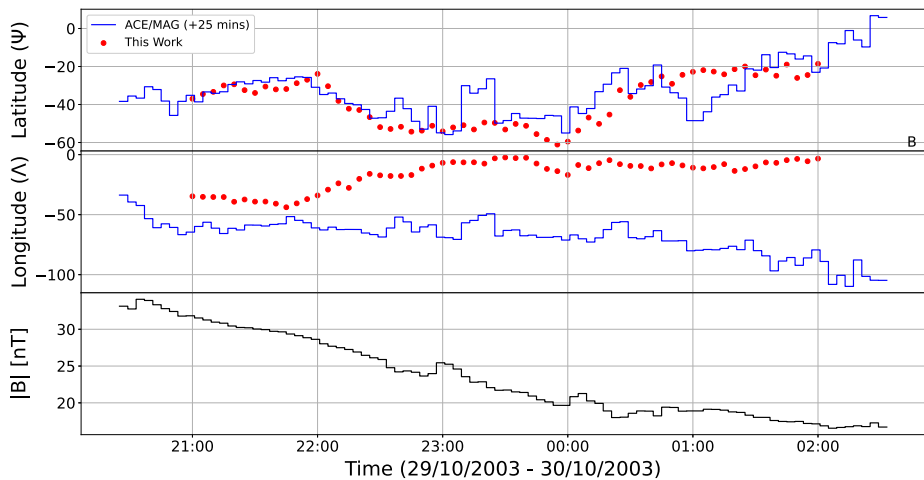


Figure 16 Similar to Figure 15 but for GLE #66.

law spectrum. Also, a nearly isotropic angular distribution of SEPs was revealed for the late stage of the events. The derived SEP spectra and their evolution are consistent with the PC and DC paradigm, and (e.g., Vashenyuk, Balabin, and Gvozdevsky, 2011; Kocharov et al., 2021). Additionally, the dynamics of spectral and angular characteristics suggest possible continuous re-acceleration of the SEPs and dominating cross-field transport (for details, see Kocharov et al., 2023, and the discussion therein).

The derived spectra and angular distribution of GLEs #65 and #66 presented here provide a solid basis for further study of their origin (e.g., Anastasiadis et al., 2019; Kocharov et al., 2020; Kouloumvakos et al., 2020; Klein et al., 2022) and improve the corresponding models (e.g., Whitman et al., 2022, and references therein), specifically the high-energy range, when enough statistics of GLE-causing SEP spectra is eventually accumulated.

Acknowledgments We warmly acknowledge L. Kocharov for the fruitful discussions and valuable comments when preparing the manuscript. Part of this work was supported by the Academy of Finland (project 330063 QUASARE and 354280 GERACLIS). The work was also supported by the Horizon Europe program via project ALBATROS. We acknowledge the support of the International Space Science Institute (Bern, Switzerland), Visiting Fellowship Program, and International Teams No. 510 (SEESUP – Solar Extreme Events: Setting Up a Paradigm), No. 475 (Modeling Space Weather And Total Solar Irradiance Over The Past Century) and No. 585 (REASSESS). This work was partially supported by the National Science Fund of Bulgaria under contract KP-06-H28/4. We acknowledge all the PIs and colleagues from the neutron monitor stations, who kindly provided the data used in this analysis, namely: Alma Ata, Apatity, Athens, Baksan, Barantsburg, Calgary, Cape Schmidt, Erevan, Forth Smith, Hermanus, Inuvik, Irkutsk, Jungfraujoch, Kerguelen, Kiel, Lomnicky Štit, Magadan, McMurdo, Mexico City, Moscow, Nain, Newark, Norilsk, Novosibirsk, Oulu, Peawanuck, Potchefstroom, Rome, Sanae, South Pole, Terre Adelie, Thule, Tixie Bay, Tsumeb, Yakutsk.

Author contributions AM: coordination, analysis of events, writing of the manuscript, interpretation of the results. SK: analysis of events, writing of the manuscript, interpretation of the results. NL: analysis of events, writing of the manuscript. IU: writing of the manuscript, interpretation of the results.

Funding Open Access funding provided by University of Oulu (including Oulu University Hospital).

Data Availability No datasets were generated or analysed during the current study.

Declarations

Competing interests The authors declare no competing interests.

Open Access This article is licensed under a Creative Commons Attribution 4.0 International License, which permits use, sharing, adaptation, distribution and reproduction in any medium or format, as long as you give appropriate credit to the original author(s) and the source, provide a link to the Creative Commons licence, and indicate if changes were made. The images or other third party material in this article are included in the article's Creative Commons licence, unless indicated otherwise in a credit line to the material. If material is not included in the article's Creative Commons licence and your intended use is not permitted by statutory regulation or exceeds the permitted use, you will need to obtain permission directly from the copyright holder. To view a copy of this licence, visit <http://creativecommons.org/licenses/by/4.0/>.

References

- Adriani, O., Barbarino, G.C., Bazilevskaya, G.A., Bellotti, R., Boezio, M., Bogomolov, E.A., Bongi, M., Bonvicini, V., Bottai, S., Bruno, A., Cafagna, F., Campana, D., Carlson, P., Casolino, M., Castellini, G., De Santis, C., Di Felice, V., Galper, A.M., Karelin, A.V., Koldashov, S.V., Koldobskiy, S., Krutkov, S.Y., Kvashnin, A.N., Leonov, A., Malakhov, V., Marcelli, L., Martucci, M., Mayorov, A.G., Menn, W., Mergè, M., Mikhailov, V.V., Mocchiutti, E., Monaco, A., Munini, R., Mori, N., Osteria, G., Panico, B., Papini, P., Pearce, M., Picozza, P., Ricci, M., Ricciarini, S.B., Simon, M., Sparvoli, R., Spillantini, P., Stozhkov, Y.I., Vacchi, A., Vannuccini, E., Vasilyev, G., Voronov, S.A., Yurkin, Y.T., Zampa, G., Zampa, N.: 2017, Ten years of PAMELA in space. *Riv. Nuovo Cimento* **40**(10), 473. DOI.
- Aguilar, M., Ali Cavasonza, L., Ambrosi, G., Arruda, L., Attig, N., Barao, F., Barrin, L., Bartoloni, A., Başgeçmez-du Pree, S., Bates, J., Battiston, R., Behlmann, M., Beischer, B., Berdugo, J., Bertucci, B., Bindi, V., de Boer, W., Bollweg, K., Borgia, B., Boschini, M.J., Bourquin, M., Bueno, E.F., Burger, J., Burger, W.J., Burmeister, S., Cai, X.D., Capell, M., Casaus, J., Castellini, G., Cervelli, F., Chang, Y.H., Chen, G.M., Chen, H.S., Chen, Y., Cheng, L., Chou, H.Y., Chouridou, S., Choutko, V., Chung, C.H., Clark, C., Coignet, G., Consolandi, C., Contin, A., Corti, C., Cui, Z., Dadzie, K., Dai, Y.M., Delgado, C., Della Torre, S., Demirköz, M.B., Derome, L., Di Falco, S., Di Felice, V., Díaz, C., Dimiccoli, F., von Doetinchem, P., Dong, F., Donnini, F., Duranti, M., Egorov, A., Eline, A., Feng, J., Fiandrini, E., Fisher, P., Formato, V., Freeman, C., Galaktionov, Y., Gámez, C., García-López, R.J., Gargiulo, C., Gast, H., Gebauer, I., Gervasi, M., Giovacchini, F., Gómez-Coral, D.M., Gong, J., Goy, C., Grabski, V., Grandi, D., Graziani, M., Guo, K.H., Haino, S., Han, K.C., Hashmani, R.K., He, Z.H., Heber, B., Hsieh, T.H., Hu, J.Y., Huang, Z.C., Hungerford, W., Incagli, M., Jang, W.Y., Jia, Y., Jinchi, H., Kanishev, K., Khiali, B., Kim, G.N., Kirn, T., Konyushikhin, M., Kounina, O., Kounine, A., Koutsenko, V., Kuhlman, A., Kulemzin, A., La Vacca, G., Laudi, E., Laurenti, G., Lazzizzera, I., Lebedev, A., Lee, H.T., Lee, S.C., Leluc, C., Li, J.Q., Li, M., Li, Q., Li, S., Li, T.X., Li, Z.H., Light, C., Lin, C.H., Lippert, T., Liu, Z., Lu, S.Q., Lu, Y.S., Luebelsmeyer, K., Luo, J.Z., Lyu, S.S., Machate, F., Mañá, C., Marín, J., Marquardt, J., Martin, T., Martínez, G., Masi, N., Maurin, D., Menchaca-Rocha, A., Meng, Q., Mo, D.C., Molero, M., Mott, P., Mussolin, L., Ni, J.Q., Nikonov, N., Nozzoli, F., Oliva, A., Orcinha, M., Palermo, M., Palmonari, F., Paniccia, M., Pashnin, A., Pauluzzi, M., Pensotti, S., Phan, H.D., Plyaskin, V., Pohl, M., Porter, S., Qi, X.M., Qin, X., Qu, Z.Y., Quadrani, L., Rancoita, P.G., Rapin, D., Reina Conde, A., Rosier-Lees, S., Rozhkov, A., Rozza, D., Sagdeev, R., Schael, S., Schmidt, S.M., Schulz von Dratzig, A., Schwering, G., Seo, E.S., Shan, B.S., Shi, J.Y., Siedenburt, T., Solano, C., Song, J.W., Sonnabend, R., Sun, Q., Sun, Z.T., Tacconi, M., Tang, X.W., Tang, Z.C., Tian, J., Ting, S.C.C., Ting, S.M., Tomasetti, N., Torsti, J., Tüysüz, C., Urban, T., Usoskin, I., Vagelli, V., Väinö, R., Valente, E., Valtonen, E., Vázquez Acosta, M., Vecchi, M., Velasco, M., Vialle, J.P., Wang, L.Q., Wang, N.H., Wang, Q.L., Wang, S., Wang, X., Wang, Z.X., Wei, J., Weng, Z.L., Wu, H., Xiong, R.Q., Xu, W., Yan, Q., Yang, Y., Yi, H., Yu, Y.J., Yu, Z.Q., Zannoni, M., Zhang, C., Zhang, F., Zhang, F.Z., Zhang, J.H., Zhang, Z., Zhao, F., Zheng, Z.M., Zhuang, H.L., Zhukov, V., Zichichi, A., Zimmermann, N., Zuccon, P.: 2021, The Alpha Magnetic Spectrometer (AMS) on the International Space Station: part II – results from the first seven years. *Phys. Rep.* **894**, 1. DOI.
- Aleksandrov, L.: 1971, The Newton-Kantorovich regularized computing processes. *U.S.S.R. Comput. Math. Math. Phys.* **11**(1), 46. DOI.
- Alken, P., Thébault, E., Beggan, C.D., Amit, H., Aubert, J., Baerenzung, J., Bondar, T.N., Brown, W.J., Califf, S., Chambodut, A., Chulliat, A., Cox, G.A., Finlay, C.C., Fournier, A., Gillet, N., Grayver, A., Hammer, M.D., Holschneider, M., Huder, L., Hulot, G., Jager, T., Kloss, C., Korte, M., Kuang, W., Kuvshinov, A., Langlais, B., Läger, J.-M., Lesur, V., Livermore, P.W., Lowes, F.J., Macmillan, S., Magnes,

- W., Manda, M., Marsal, S., Matzka, J., Metman, M.C., Minami, T., Morschhauser, A., Mound, J.E., Nair, M., Nakano, S., Olsen, N., Pavón-Carrasco, F.J., Petrov, V.G., Ropp, G., Rother, M., Sabaka, T.J., Sanchez, S., Saturnino, D., Schnepf, N.R., Shen, X., Stolle, C., Tangborn, A., Tøffner-Clausen, L., Toh, H., Torta, J.M., Varner, J., Vervelidou, F., Vigneron, P., Wardinski, I., Wicht, J., Woods, A., Yang, Y., Zeren, Z., Zhou, B.: 2021, International geomagnetic reference field: the thirteenth generation. *Earth Planets Space* **73**(1), 49. DOI.
- Anastasiadis, A., Lario, D., Papaioannou, A., Kouloumvakos, A., Vourlidis, A.: 2019, Solar energetic particles in the inner heliosphere: status and open questions. *Phil. Trans. Roy. Soc., Math. Phys. Eng. Sci.* **377**(2148), 20180100. DOI.
- Andriopoulou, M., Mavromichalaki, H., Plainaki, C., Belov, A., Eroshenko, E.: 2011a, Intense ground-level enhancements of solar cosmic rays during the last solar cycles. *Solar Phys.* **269**(1), 155.
- Andriopoulou, M., Mavromichalaki, H., Preka-Papadema, P., Plainaki, C., Belov, A., Eroshenko, E.: 2011b, Solar activity and the associated ground level enhancements of solar cosmic rays during solar cycle 23. *Astrophys. Space Sci. Trans.* **7**(4), 439.
- Aschwanden, M.: 2012, GeV particle acceleration in solar flares and ground level enhancement (GLE) events. *Space Sci. Rev.* **171**(1–4), 3. DOI.
- Aster, R.C., Borchers, B., Thurber, C.H.: 2005, *Parameter Estimation and Inverse Problems*, Elsevier, New York. ISBN 0-12-065604-3.
- Aurass, H., Mann, G., Rausche, G., Warmuth, A.: 2006, The GLE on Oct. 28, 2003 – radio diagnostics of relativistic electron and proton injection. *Astron. Astrophys.* **457**(2), 681. DOI.
- Balabin, Y.V.: 2023, Analysis of anomalous event GLE 66 on October 29, 2003. *Bull. Russ. Acad. Sci., Phys.* **87**(2), 228.
- Beatty, J.J., Matthews, J.H., Wakely, S.P.: 2018, Cosmic rays. In: *Review of Particle Physics*, Physical Review D **98**, 030001, 424. DOI.
- Bombardieri, D.J., Duldig, M.L., Michael, K.J., Humble, J.E.: 2006, Relativistic proton production during the 2000 July 14 solar event: the case for multiple source mechanisms. *Astrophys. J.* **644**(1), 565.
- Bruno, A., Bazilevskaya, G.A., Boezio, M., Christian, E.R., de Nolfo, G.A., Martucci, M., Merge', M., Mikhailov, V.V., Munini, R., Richardson, I.G., Ryan, J.M., Stochaj, S., Adriani, O., Barbarino, G.C., Bellotti, R., Bogomolov, E.A., Bongi, M., Bonvicini, V., Bottai, S., Cafagna, F., Campana, D., Carlson, P., Casolino, M., Castellini, G., Santis, C.D., Felice, V.D., Galper, A.M., Karelin, A.V., Koldashov, S.V., Koldobskiy, S., Krutkov, S.Y., Kvashnin, A.N., Leonov, A., Malakhov, V., Marcelli, L., Mayorov, A.G., Menn, W., Mocchiutti, E., Monaco, A., Mori, N., Osteria, G., Panico, B., Papini, P., Pearce, M., Picozza, P., Ricci, M., Ricciarini, S.B., Simon, M., Sparvoli, R., Spillantini, P., Stozhkov, Y.I., Vacchi, A., Vanuccini, E., Vasilyev, G.I., Voronov, S.A., Yurkin, Y.T., Zampa, G., Zampa, N.: 2018, Solar energetic particle events observed by the PAMELA mission. *Astrophys. J.* **862**(2), 97. DOI.
- Bütikofer, R.: 2018, Cosmic ray particle transport in the Earth's magnetosphere. In: *Solar Particle Radiation Storms Forecasting and Analysis, the HESPERIA HORIZON 2020 Project and Beyond*, Springer, Cham, Chapter 5. ISBN 978-3-319-60051-2.
- Bütikofer, R., Flückiger, E.O.: 2015, What are the causes for the spread of GLE parameters deduced from NM data? *J. Phys. Conf. Ser.* **632**(1), 012053. DOI.
- Bütikofer, R., Flückiger, E.O., Desorgher, L., Moser, M.R., Pirard, B.: 2009, The solar cosmic ray ground-level enhancements on 20 January, 2005 and 13 December, 2006. *Adv. Space Res.* **43**(4), 499.
- Caballero-Lopez, R.A., Moraal, H.: 2004, Limitations of the force field equation to describe cosmic ray modulation. *J. Geophys. Res.* **109**, A01101. DOI.
- Chupp, E.L., Ryan, J.M.: 2009, High energy neutron and pion-decay gamma-ray emissions from solar flares. *Res. Astron. Astrophys.* **9**(1), 11. DOI.
- Clem, J.M.: 1997, Contribution of obliquely incident particles to neutron monitor counting rate. *J. Geophys. Res.* **102**, 919.
- Cooke, D.J., Humble, J.E., Shea, M.A., Smart, D.F., Lund, N., Rasmussen, I.L., Byrnak, B., Goret, P., Petrou, N.: 1991, On cosmic-ray cutoff terminology. *Nuovo Cimento C* **14**(3), 213. DOI.
- Cramp, J.L., Humble, J.E., Duldig, M.L.: 1994, The cosmic ray ground-level enhancement of 24 October, 1989. *Publ. Astron. Soc. Aust.* **11**(1), 28.
- Cramp, J.L., Duldig, M.L., Flückiger, E.O., Humble, J.E., Shea, M.A., Smart, D.F.: 1997, The October 22, 1989, solar cosmic ray enhancement: an analysis of the anisotropy spectral characteristics. *J. Geophys. Res.* **102**(A11), 24237. DOI.
- Dalla, S., Marsh, M.S., Kelly, J., Laitinen, T.: 2013, Solar energetic particle drifts in the Parker spiral. *J. Geophys. Res. Space Phys.* **118**(10), 5979. DOI.
- Debrunner, H., Flückiger, E.O., Gradel, H., Lockwood, J.A., McGuire, R.E.: 1988, Observations related to the acceleration, injection, and interplanetary propagation of energetic protons during the solar cosmic ray event on February 16, 1984. *J. Geophys. Res.* **93**(A7), 7206.

- Dennis, J.E., Schnabel, R.B.: 1996, *Numerical Methods for Unconstrained Optimization and Nonlinear Equations*, Prentice-Hall, Englewood Cliffs. ISBN 13-978-0-898713-64-0.
- Desai, M., Giacalone, J.: 2016, Large gradual solar energetic particle events. *Living Rev. Solar Phys.* **13**(1), 3. DOI.
- Desorgher, L., Flückiger, E.O., Gurtner, M., Moser, M.R., Bütikofer, R.: 2005, A GEANT4 code for computing the interaction of cosmic rays with the Earth's atmosphere. *Int. J. Mod. Phys. A* **20**(A11), 6802. DOI.
- Dorman, L.: 2006, *Cosmic Ray Interactions, Propagation, and Acceleration in Space Plasmas, Astrophysics and Space Science Library* **339**, Springer, Dordrecht. ISBN 13-978-1-4020-5100-5.
- Dorman, L.I., Velinov, P.I.Y., Mishev, A.: 2022, Global planetary ionization maps in Regener–Pfotzer cosmic ray maximum for GLE 66 during magnetic superstorm of 29–31 October, 2003. *Adv. Space Res.* **70**(9), 2593.
- Ellison, D.C., Ramaty, R.: 1985, Shock acceleration of electrons and ions in solar flares. *Astrophys. J.* **298**, 400. DOI.
- Engelbrecht, N.E., Effenberger, F., Florinski, V., Potgieter, M.S., Ruffolo, D., Chhiber, R., Usmanov, A.V., Rankin, J.S., Els, P.L.: 2022, Theory of cosmic ray transport in the heliosphere. *Space Sci. Rev.* **218**(4), 33. DOI.
- Engl, H.W., Hanke, M., Neubauer, A.: 1996, *Regularization of Inverse Problems*, Kluwer Academic, Dordrecht. ISBN 0792341570, 9780792341574.
- Forbush, S.E.: 1946, Three unusual cosmic-ray increases possibly due to charged particles from the Sun. *Phys. Rev.* **70**(9–10), 771. DOI.
- Forbush, S.E.: 1958, Cosmic-ray intensity variations during two solar cycles. *J. Geophys. Res.* **63**(4), 651.
- Forbush, S.E., Stinchcomb, T.B., Schein, M.: 1950, The extraordinary increase of cosmic-ray intensity on November 19, 1949. *Phys. Rev.* **79**(3), 501. DOI.
- Gil, A., Usoskin, I.G., Kovaltsov, G.A., Mishev, A.L., Corti, C., Bindi, V.: 2015, Can we properly model the neutronmonitor count rate? *J. Geophys. Res.* **120**, 7172.
- Gopalswamy, N., Barbieri, L., Cliver, E.W., Lu, G., Plunkett, S.P., Skoug, R.M.: 2005, Introduction to violent Sun–Earth connection events of October–November 2003. *J. Geophys. Res. Space Phys.* **110**(A9), A09S00. DOI.
- Gopalswamy, N., Xie, H., Yashiro, S., Akiyama, S., Mäkelä, P., Usoskin, I.G.: 2012, Properties of ground level enhancement events and the associated solar eruptions during solar cycle 23. *Space Sci. Rev.* **171**(1–4), 23. DOI.
- Grechnev, V.V., Uralov, A.M., Slemzin, V.A., Chertok, I.M., Filippov, B.P., Rudenko, G.V., Temmer, M.: 2014, A challenging solar eruptive event of 18 November, 2003 and the causes of the 20 November geomagnetic superstorm. I. Unusual history of an eruptive filament. *Solar Phys.* **289**(1), 289. DOI.
- Hatton, C.: 1971, The neutron monitor. In: *Progress in Elementary Particle and Cosmic-Ray Physics X*, North-Holland, Amsterdam, Chapter 1.
- Hatton, C., Carmichael, H.: 1964, Experimental investigation of the NM-64 neutron monitor. *Can. J. Phys.* **42**, 2443.
- Herbst, K., Kopp, A., Heber, B., Steinhilber, F., Fichtner, H., Scherer, K., Matthiä, D.: 2010, On the importance of the local interstellar spectrum for the solar modulation parameter. *J. Geophys. Res., Atmos.* **115**(D1), D00I20.
- Himmelblau, D.M.: 1972, *Applied Nonlinear Programming*, McGraw-Hill, New York. ISBN 978-0070289215.
- Hovestadt, D., Hilchenbach, M., Bürgi, A., Klecker, B., Laeverenz, P., Scholer, M., Grünwaldt, H., Axford, W.I., Livi, S., Marsch, E., Wilken, B., Winterhoff, H.P., Ipavich, F.M., Bedini, P., Coplan, M.A., Galvin, A.B., Gloeckler, G., Bochsler, P., Balsiger, H., Fischer, J., Geiss, J., Kallenbach, R., Wurz, P., Reiche, K.-U., Gliem, F., Judge, D.L., Ogawa, H.S., Hsieh, K.C., Möbius, E., Lee, M.A., Managadze, G.G., Verigin, M.I., Neugebauer, M.: 1995, Celiac – charge, element and isotope analysis system for SOHO. *Solar Phys.* **162**(1–2), 441. DOI.
- Huber, R.: 2019, *Variational Regularization for Systems of Inverse Problems: Tikhonov Regularization with Multiple Forward Operators*, Springer, Wiesbaden. ISBN 9783658253899.
- Klassen, A., Krucker, S., Kunow, H., Müller-Mellin, R., Wimmer-Schweingruber, R., Mann, G., Posner, A.: 2005, Solar energetic electrons related to the 28 October, 2003 flare. *J. Geophys. Res. Space Phys.* **110**(A9), A09S04. DOI.
- Klein, K.-L., Musset, S., Vilmer, N., Briand, C., Krucker, S., Francesco Battaglia, A., Dresing, N., Palmroos, C., Gary, D.E.: 2022, The relativistic solar particle event on 28 October, 2021: evidence of particle acceleration within and escape from the solar corona. *Astron. Astrophys.* **663**, A173. DOI.
- Kocharov, L., Pohjolainen, S., Mishev, A., Reiner, M.J., Lee, J., Laitinen, T., Didkovsky, L.V., Pizzo, V.J., Kim, R., Klassen, A., Karlicky, M., Cho, K.-S., Gary, D.E., Usoskin, I., Valtonen, E., Vainio, R.: 2017, Investigating the origins of two extreme solar particle events: proton source profile and associated electromagnetic emissions. *Astrophys. J.* **839**(2), 79. DOI.

- Kocharov, L., Pesce-Rollins, M., Laitinen, T., Mishev, A., Kühl, P., Klassen, A., Jin, M., Omodei, N., Longo, F., Webb, D.F., Cane, H.V., Heber, B., Vainio, R., Usoskin, I.: 2020, Interplanetary protons versus interacting protons in the 2017 September 10 solar eruptive event. *Astrophys. J.* **890**(1), 13. DOI.
- Kocharov, L., Omodei, N., Mishev, A., Pesce-Rollins, M., Longo, F., Yu, S., Gary, D.E., Vainio, R., Usoskin, I.: 2021, Multiple sources of solar high-energy protons. *Astrophys. J.* **915**(1), 12. DOI.
- Kocharov, L., Mishev, A., Riihonen, E., Vainio, R., Usoskin, I.: 2023, A comparative study of ground level enhancement events of solar energetic particles. *Astrophys. J.* **958**(2), 122. DOI.
- Koldobskiy, S.A., Kovaltsov, G.A., Usoskin, I.G.: 2018, Effective rigidity of a polar neutron monitor for recording ground-level enhancements. *Solar Phys.* **293**(7), 110. DOI.
- Koldobskiy, S., Mishev, A.: 2022, Fluences of solar energetic particles for last three GLE events: comparison of different reconstruction methods. *Adv. Space Res.* **70**(9), 2585. DOI.
- Koldobskiy, S.A., Bindi, V., Corti, C., Kovaltsov, G.A., Usoskin, I.G.: 2019a, Validation of the neutron monitor yield function using data from AMS-02 experiment 2011–2017. *J. Geophys. Res. Space Phys.* **124**, 2367. DOI.
- Koldobskiy, S., Kovaltsov, G.A., Mishev, A., Usoskin, I.G.: 2019b, New method of assessment of the integral fluence of solar energetic (> 1 GV rigidity) particles from neutron monitor data. *Solar Phys.* **294**, 94. DOI.
- Koldobskiy, S., Raukunen, O., Vainio, R., Kovaltsov, G.A., Usoskin, I.: 2021, New reconstruction of event-integrated spectra (spectral fluences) for major solar energetic particle events. *Astron. Astrophys.* **647**, A132. DOI.
- Kouloumvakos, A., Rouillard, A.P., Share, G.H., Plotnikov, I., Murphy, R., Papaioannou, A., Wu, Y.: 2020, Evidence for a coronal shock wave origin for relativistic protons producing solar gamma-rays and observed by neutron monitors at Earth. *Astrophys. J.* **893**(1), 76. DOI.
- Kudela, K., Bučik, R., Bobik, P.: 2008, On transmissivity of low energy cosmic rays in disturbed magnetosphere. *Adv. Space Res.* **42**(7), 1300.
- Kudela, K., Usoskin, I.: 2004, On magnetospheric transmissivity of cosmic rays. *Czechoslov. J. Phys.* **54**(2), 239.
- Laitinen, T., Dalla, S.: 2017, Energetic particle transport across the mean magnetic field: before diffusion. *Astrophys. J.* **834**(2), 127. DOI.
- Laitinen, T., Dalla, S., Waterfall, C.O.G., Hutchinson, A.: 2023, Solar energetic particle event onsets at different heliolongitudes: the effect of turbulence in Parker spiral geometry. *Astron. Astrophys.* **673**, L8. DOI.
- Larsen, N., Mishev, A., Usoskin, I.: 2023, A new open-source geomagnetosphere propagation tool (OTSO) and its applications. *J. Geophys. Res. Space Phys.* **128**(3), e2022JA031061. DOI.
- Levenberg, K.: 1944, A method for the solution of certain non-linear problems in least squares. *Q. Appl. Math.* **2**, 164.
- Li, C., Tang, Y.H., Dai, Y., Fang, C., Vial, J.-C.: 2007, Flare magnetic reconnection and relativistic particles in the 2003 October 28 event. *Astron. Astrophys.* **472**(1), 283. DOI.
- Liu, Y., Hayashi, K.: 2006, The 2003 October–November fast halo coronal mass ejections and the large-scale magnetic field structures. *Astrophys. J.* **640**(21), 1135. DOI.
- Marquardt, D.: 1963, An algorithm for least-squares estimation of nonlinear parameters. *SIAM J. Appl. Math.* **11**(2), 431.
- Mavrodiev, S.C., Mishev, A.L., Stamenov, J.N.: 2004, A method for energy estimation and mass composition determination of primary cosmic rays at the Chacaltaya observation level based on the atmospheric Cherenkov light technique. *Nucl. Instrum. Methods Phys. Res., Sect. A, Accel. Spectrom. Detect. Assoc. Equip.* **530**(3), 359. DOI.
- Mavromichalaki, H., Papaioannou, A., Plainaki, C., Sarlanis, C., Souvatzoglou, G., Gerontidou, M., Papailiou, M., Eroshenko, E., Belov, A., Yanke, V., Flückiger, E.O., Büttikofer, R., Parisi, M., Storini, M., Klein, K.-L., Fuller, N., Steigies, C.T., Rother, O.M., Heber, B., Wimmer-Schweingruber, R.F., Kudela, K., Strharsky, I., Langer, R., Usoskin, I., Ibragimov, A., Chilingaryan, A., Hovsepian, G., Reymers, A., Yeghikyan, A., Kryakunova, O., Dryn, E., Nikolayevskiy, N., Dorman, L., Pustil'Nik, L.: 2011, Applications and usage of the real-time neutron monitor database. *Adv. Space Res.* **47**, 2210.
- Miroshnichenko, L.I.: 2018, Retrospective analysis of GLEs and estimates of radiation risks. *J. Space Weather Space Clim.* **8**, A52. DOI.
- Miroshnichenko, L.I., Klein, K.-L., Trottet, G., Lantos, P., Vashenyuk, E.V., Balabin, Y.V., Gvozdevsky, B.B.: 2005, Relativistic nucleon and electron production in the 2003 October 28 solar event. *J. Geophys. Res. Space Phys.* **110**(A9), A09S08. DOI.
- Mishev, A.L.: 2023, Application of the global neutron monitor network for assessment of spectra and anisotropy and the related terrestrial effects of strong SEPs. *J. Atmos. Solar-Terr. Phys.* **243**, 106021. DOI.

- Mishev, A.L., Kocharov, L.G., Usoskin, I.G.: 2014, Analysis of the ground level enhancement on 17 May, 2012 using data from the global neutron monitor network. *J. Geophys. Res.* **119**, 670.
- Mishev, A., Mavrodiiev, S., Stamenov, J.: 2005, Gamma rays studies based on atmospheric Cherenkov technique at high mountain altitude. *Int. J. Mod. Phys. A* **20**(29), 7016. DOI.
- Mishev, A., Poluianov, S.: 2021, About the altitude profile of the atmospheric cut-off of cosmic rays: new revised assessment. *Solar Phys.* **296**(8), 129. DOI.
- Mishev, A., Usoskin, I.: 2016a, Analysis of the ground level enhancements on 14 July, 2000 and on 13 December, 2006 using neutron monitor data. *Solar Phys.* **291**(4), 1225. DOI.
- Mishev, A., Usoskin, I.: 2016b, Erratum to: "Analysis of the ground level enhancements on 14 July, 2000 and on 13 December, 2006 using neutron monitor data". *Solar Phys.* **291**(4), 1579. DOI.
- Mishev, A.L., Usoskin, I.G.: 2018, Assessment of the radiation environment at commercial jet-flight altitudes during GLE 72 on 10 September, 2017 using neutron monitor data. *Space Weather* **16**(12), 1921. DOI.
- Mishev, A., Velinov, P.I.Y.: 2011, Normalized ionization yield function for various nuclei obtained with full Monte Carlo simulations. *Adv. Space Res.* **48**(1), 19.
- Mishev, A., Usoskin, I., Raukunen, O., Paassilta, M., Valtonen, E., Kocharov, L., Vainio, R.: 2018, First analysis of GLE 72 event on 10 September 2017: spectral and anisotropy characteristics. *Solar Phys.* **293**, 136. DOI.
- Mishev, A.L., Koldobskiy, S.A., Kovaltsov, G.A., Gil, A., Usoskin, I.G.: 2020, Updated neutron-monitor yield function: bridging between in situ and ground-based cosmic ray measurements. *J. Geophys. Res. Space Phys.* **125**(2), e2019JA027433. DOI.
- Mishev, A.L., Koldobskiy, S.A., Kocharov, L.G., Usoskin, I.G.: 2021b, GLE #67 event on 2 November, 2003: an analysis of the spectral and anisotropy characteristics using verified yield function and detrended neutron monitor data. *Solar Phys.* **296**(5), 79. DOI.
- Mishev, A.L., Koldobskiy, S.A., Usoskin, I.G., Kocharov, L.G., Kovaltsov, G.A.: 2021a, Application of the verified neutron monitor yield function for an extended analysis of the GLE #71 on 17 May, 2012. *Space Weather* **19**(2), e2020SW002626. DOI.
- Mishev, A.L., Kocharov, L.G., Koldobskiy, S.A., Larsen, N., Riihonen, E., Vainio, R., Usoskin, I.G.: 2022, High-resolution spectral and anisotropy characteristics of solar protons during the GLE N° 73 on 28 October, 2021 derived with neutron-monitor data analysis. *Solar Phys.* **297**(7), 88. DOI.
- Moraal, H., McCracken, K.G.: 2012, The time structure of ground level enhancements in solar cycle 23. *Space Sci. Rev.* **171**(1–4), 85. DOI.
- More, G., Garbow, B.S., Hillstrome, K.E.: 1980, User guide for minpack-1. Report ANL 80-74, Argonne National Laboratory, Downers Grove Township, IL, USA.
- Nevalainen, J., Usoskin, I., Mishev, A.: 2013, Eccentric dipole approximation of the geomagnetic field: application to cosmic ray computations. *Adv. Space Res.* **52**(1), 22. DOI.
- Nuntiyakul, W., Sáiz, A., Ruffolo, D., Mangeard, P.-S., Evenson, P., Bieber, J.W., Clem, J., Pyle, R., Duldig, M.L., Humble, J.E.: 2018, Bare neutron counter and neutron monitor response to cosmic rays during a 1995 latitude survey. *J. Geophys. Res. Space Phys.* **123**(9), 7181. DOI.
- Papaoiannou, A., Sandberg, I., Anastasiadis, A., Kouloumvakos, A., Georgoulis, M.K., Tziotziou, K., Tsiropoula, G., Jiggins, P., Hilgers, A.: 2016, Solar flares, coronal mass ejections and solar energetic particle event characteristics. *J. Space Weather Space Clim.* **6**, A42. DOI.
- Papaoiannou, A., Kouloumvakos, A., Mishev, A., Vainio, R., Usoskin, I., Herbst, K., Rouillard, A.P., Anastasiadis, A., Gieseler, J., Wimmer-Schweingruber, R., Kühl, P.: 2022, The first ground level enhancement of solar cycle 25 on 28 October, 2021. *Astron. Astrophys.* **660**, L5. DOI.
- Poluianov, S.V., Usoskin, I.G., Mishev, A.L., Shea, M.A., Smart, D.F.: 2017, Gle and sub-GLE redefinition in the light of high-altitude polar neutron monitors. *Solar Phys.* **292**(11), 176. DOI.
- Pulkkinen, A., Lindahl, S., Viljanen, A., Pirjola, R.: 2005, Geomagnetic storm of 29–31 October, 2003: geomagnetically induced currents and their relation to problems in the Swedish high-voltage power transmission system. *Space Weather* **3**(8), S08C03.
- Raukunen, O., Vainio, R., Tyllka, A.J., Dietrich, W.F., Jiggins, P., Heynderickx, D., Dierckx, M., Crosby, N., Ganse, U., Siipola, R.: 2018, Two solar proton fluence models based on ground level enhancement observations. *J. Space Weather Space Clim.* **8**, A04. DOI.
- Reames, D.V.: 2013, The two sources of solar energetic particles. *Space Sci. Rev.* **175**(1–4), 53. DOI.
- Schuster, T., Kaltenbacher, B., Hofmann, B., Kazimierski, K.: 2012, *Regularization Methods in Banach Spaces, Johann Radon Institute for Computational and Applied Mathematics; Radon Series on Computational and Applied Mathematics*, de Gruyter, Berlin. ISBN 9783110255249.
- Shea, M.A., Smart, D.F.: 1982, Possible evidence for a rigidity-dependent release of relativistic protons from the solar corona. *Space Sci. Rev.* **32**, 251. DOI.
- Shea, M.A., Smart, D.F.: 2000, Fifty years of cosmic radiation data. *Space Sci. Rev.* **93**(1–2), 229. DOI.
- Simpson, J.: 1957, Cosmic-radiation neutron intensity monitor. *Ann. Int. Geophys. Year* **4**, 351.

- Simpson, J.: 2000, The cosmic ray nucleonic component: the invention and scientific uses of the neutron monitor. *Space Sci. Rev.* **93**, 11. DOI.
- Simpson, J., Fonger, W., Treiman, S.: 1953, Cosmic radiation intensity-time variation and their origin. I. Neutron intensity variation method and meteorological factors. *Phys. Rev.* **90**, 934.
- Smart, D.F., Shea, M.A., Flückiger, E.O.: 2000, Magnetospheric models and trajectory computations. *Space Sci. Rev.* **93**(1), 305.
- Smith, C.W., L'Heureux, J., Ness, N.F., Acuña, M.H., Burlaga, L.F., Scheifele, J.: 1998, The ace magnetic fields experiment. *Space Sci. Rev.* **86**(1–4), 613. DOI.
- Stoker, P.H., Dorman, L.I., Clem, J.M.: 2000, Neutron monitor design improvements. *Space Sci. Rev.* **93**(1–2), 361.
- Strutz, T.: 2011, *Data Fitting and Uncertainty: A Practical Introduction to Weighted Least Squares and Beyond*, Vieweg+Teubner. Springer, Wiesbaden. ISBN 9783834810229.
- Tikhonov, A.N., Goncharov, A.V., Stepanov, V.V., Yagola, A.G.: 1995, *Numerical Methods for Solving Ill-Posed Problems*, Kluwer Academic, Dordrecht. ISBN 978-90-481-4583-6.
- Tsyganenko, N.A.: 1989, A magnetospheric magnetic field model with a warped tail current sheet. *Planet. Space Sci.* **37**(1), 5.
- Tsyganenko, N.A.: 2002, A model of the near magnetosphere with a dawn–dusk asymmetry. *J. Geophys. Res. Space Phys.* **107**(A8), SMP 12-1. DOI.
- Tylka, A., Dietrich, W.: 2009, A new and comprehensive analysis of proton spectra in ground-level enhanced (GLE) solar particle events. In: *Proc. of 31th ICRC, Poland, Lodz, 7–15 July, 2009*, 0273.
- Usoskin, I., Kovaltsov, G.: 2006, Cosmic ray induced ionization in the atmosphere: full modeling and practical applications. *J. Geophys. Res.* **111**, D21206.
- Usoskin, I., Alanko-Huotari, K., Kovaltsov, G., Mursula, K.: 2005, Heliospheric modulation of cosmic rays: monthly reconstruction for 1951–2004. *J. Geophys. Res.* **110**, A12108. DOI.
- Usoskin, I.G., Ibragimov, A., Shea, M.A., Smart, D.F.: 2015, Database of ground level enhancements (GLE) of high energy solar proton events. In: *Proceedings of Science, Proc. of 34th ICRC, Hague, The Netherlands, 30 July–6 August 2015*, 054.
- Usoskin, I.G., Gil, A., Kovaltsov, G.A., Mishev, A.L., Mikhailov, V.V.: 2017, Heliospheric modulation of cosmic rays during the neutron monitor era: calibration using PAMELA data for 2006–2010. *J. Geophys. Res.* **122**, 3875. DOI.
- Usoskin, I., Koldobskiy, S., Kovaltsov, G.A., Gil, A., Usoskina, I., Willamo, T., Ibragimov, A.: 2020b, Revised GLE database: fluences of solar energetic particles as measured by the neutron-monitor network since 1956. *Astron. Astrophys.* **640**, 2038272. DOI.
- Usoskin, I.G., Koldobskiy, S.A., Kovaltsov, G.A., Rozanov, E.V., Sukhodolov, T.V., Mishev, A.L., Mironova, I.A.: 2020a, Revisited reference solar proton event of 23 February, 1956: assessment of the cosmogenic-isotope method sensitivity to extreme solar events. *J. Geophys. Res. Space Phys.* **125**(6), e2020JA027921. DOI.
- Väisänen, P., Usoskin, I., Kähkönen, R., Koldobskiy, S., Mursula, K.: 2023, Revised reconstruction of the heliospheric modulation potential for 1964–2022. *J. Geophys. Res. Space Phys.* **128**(4), e2023JA031352. DOI.
- van den Berg, J., Strauss, D.T., Effenberger, F.: 2020, A primer on focused solar energetic particle transport: basic physics and recent modelling results. *Space Sci. Rev.* **216**(8), 146. DOI.
- Vashenyuk, E.V., Balabin, Y.V., Gvozdevsky, B.B.: 2011, Features of relativistic solar proton spectra derived from ground level enhancement events (GLE) modeling. *Astrophys. Space Sci. Trans.* **7**(4), 459. DOI.
- Vashenyuk, E.V., Balabin, Y.V., Perez-Peraza, J., Gallegos-Cruz, A., Miroshnichenko, L.I.: 2006, Some features of the sources of relativistic particles at the sun in the solar cycles 21–23. *Adv. Space Res.* **38**(3), 411. DOI.
- Vos, E.E., Potgieter, M.S.: 2015, New modeling of galactic proton modulation during the minimum of solar cycle 23/24. *Astrophys. J.* **815**, 119. DOI.
- Waterfall, C.O.G., Dalla, S., Laitinen, T., Hutchinson, A., Marsh, M.: 2022, Modeling the transport of relativistic solar protons along a heliospheric current sheet during historic GLE events. *Astrophys. J.* **934**(1), 82. DOI.
- Waterfall, C.O.G., Dalla, S., Raukunen, O., Heynderickx, D., Jiggins, P., Vainio, R.: 2023, High energy solar particle events and their relationship to associated flare, CME and GLE parameters. *Space Weather* **21**(3), e2022SW003334. DOI.
- Whitman, K., Egeland, R., Richardson, I.G., Allison, C., Quinn, P., Barzilla, J., Kitiashvili, I., Sadykov, V., Bain, H.M., Dierckx, M., Mays, M.L., Tadesse, T., Lee, K.T., Semones, E., Luhmann, J.G., Núñez, M., White, S.M., Kahler, S.W., Ling, A.G., Smart, D.F., Shea, M.A., Tenishev, V., Boubrahimi, S.F., Aydin, B., Martens, P., Angryk, R., Marsh, M.S., Dalla, S., Crosby, N., Schwadron, N.A., Kozarev, K., Gorby, M., Young, M.A., Laurenza, M., Cliver, E.W., Alberti, T., Stumpo, M., Benella, S., Papaioannou, A., Anastasiadis, A., Sandberg, I., Georgoulis, M.K., Ji, A., Kempton, D., Pandey, C., Li, G., Hu, J.,

- Zank, G.P., Lavasa, E., Giannopoulos, G., Falconer, D., Kadadi, Y., Fernandes, I., Dayeh, M.A., Muñoz-Jaramillo, A., Chatterjee, S., Moreland, K.D., Sokolov, I.V., Roussev, I.I., Taktakishvili, A., Effenberger, F., Gombosi, T., Huang, Z., Zhao, L., Wijsen, N., Aran, A., Poedts, S., Kouloumvakos, A., Paassilta, M., Vainio, R., Belov, A., Eroshenko, E.A., Abunina, M.A., Abunin, A.A., Balch, C.C., Malandraki, O., Karavolos, M., Heber, B., Labrenz, J., Köhl, P., Kosovichev, A.G., Oria, V., Nita, G.M., Illarionov, E., O'Keefe, P.M., Jiang, Y., Ferreira, S.H., Ali, A., Paouris, E., Aminimalragia-Giamini, S., Jiggins, P., Jin, M., Lee, C.O., Palmerio, E., Bruno, A., Kasapis, S., Wang, X., Chen, Y., Sanahuja, B., Lario, D., Jacobs, C., Strauss, D.T., Steyn, R., van den Berg, J., Swalwell, B., Waterfall, C., Nedal, M., Miteva, R., Dechev, M., Zucca, P., Engell, A., Maze, B., Farmer, H., Kerber, T., Barnett, B., Loomis, J., Grey, N., Thompson, B.J., Linker, J.A., Caplan, R.M., Downs, C., Török, T., Lionello, R., Titov, V., Zhang, M., Hosseinzadeh, P.: 2022, Review of solar energetic particle models. *Adv. Space Res.* [DOI](#).
- Zurbuchen, T.H., Gloeckler, G., Ipavich, F., Raines, J., Smith, C.W., Fisk, L.A.: 2004, On the fast coronal mass ejections in October/November 2003: ACE-SWICS results. *Geophys. Res. Lett.* **31**(11), L11805. [DOI](#).

Publisher's Note Springer Nature remains neutral with regard to jurisdictional claims in published maps and institutional affiliations.